4-2014

# An Iron Polypyridyl Electrocatalyst for Hydrogen Generation in Aqueous Solutions

Gannon P. Connor
*College of William and Mary*

# An Iron Polypyridyl Electrocatalyst for Hydrogen Generation in Aqueous Solutions

A thesis submitted in partial fulfillment of the requirement
for the degree of Bachelors of Science in Department of Chemistry from
The College of William and Mary

By

Gannon P. Connor

**Accepted for _____**

_____
**William R. McNamara**

_____
**James P. Barber**

_____
**Robert D. Pike**

_____
**Kristin Wustholz**

Williamsburg, VA
**April 29, 2014**

# Table of Contents

## Acknowledgements

I would like to thank Dr. William McNamara for his mentorship and guidance throughout the course of this project. I consider joining your group one of the best decisions of my undergraduate career, and I would not be even close to where I am without your encouragement and assistance. Thank you for training me in both the scientific method and how to be effective in the laboratory. Thank you for giving me the opportunity to help write a manuscript on this project and for your patience when I was slow on results and follow-ups. I sincerely appreciate the devotion you have shown to my development as a chemist and a scholar.

I would also like to thank the fantastic chemistry faculty at William and Mary, who inspired me to pursue a career in chemistry. I especially want to thank Dr. Robert Pike for introducing me to the incredibly interesting field of organometallic chemistry and Dr. Kristin Wustholz for putting up with me for three (!) semesters of physical chemistry. Advanced Inorganic and Advanced Physical Chemistry remain my favorite classes taken to date, and it is no coincidence that I am pursuing a Ph. D. in a combination of these fields.

I am also grateful for Dr. Jillian Dempsey of UNC and the Dempsey group who helped me better understand the fundamental concepts of electrochemistry. This knowledge was essential to allowing me to correctly interpret the results of the numerous cyclic voltammetry experiments that I conducted.

Additionally, I would like to thank Dr. Pike, Dr. Wustholz, and Dr. Jim Barber for serving on my committee. I appreciate your time, consideration, and mentorship.

I have had an overwhelmingly positive experience with the McNamara group, and I would like to thank all of my peers for their help and feedback. I give special thanks to Matt Van Dongen, my late night lab partner, and Kathryn Mayer for her significant contributions to this project.

Finally, thank you to the William and Mary Charles Center and the extremely generous donors who supported my Honors Fellowship. I hope you find my project as interesting as I do, and I couldn't have done it without you!

## List of Figures and Tables

## Abstract

An iron polypyridyl complex has been synthesized, characterized, and analyzed as an electrocatalyst for proton reduction. The complex is highly active in both organic and aqueous solutions, exhibiting a catalytic rate of $1200s^{-1}$ at 660 mV overpotential in acetonitrile and $3500s^{-1}$ at 800 mV overpotential in 1:1 water:acetonitrile. These rates establish the complex as one of the most active iron electrocatalyst for proton reduction reported at this time. Additionally, the catalyst can generate hydrogen from aqueous buffer solutions between pH= 3-6, with a turnover number of 23 over one hour at a Faradaic efficiency of 98%.

# Introduction

## The Global Energy Crisis

In 2013, the global energy consumption was 577 x $10^{18}$ J, or 18.3 TW. According to projections from the U.S. Energy Information Administration, the global rate of energy consumption will increase to 27.4 TW by 2040, at an annual rate of close to 1.5%.[1] Our current energy consumption relies heavily on the combustion of fossil fuels such as liquid fuels, coal, and natural gas. Fig. 1 illustrates the global reliance on these hydrocarbon fuels over other energy sources such as nuclear, hydroelectric, and solar methods. Fossil fuels are expected to account for approximately 80% of world energy use through 2040.

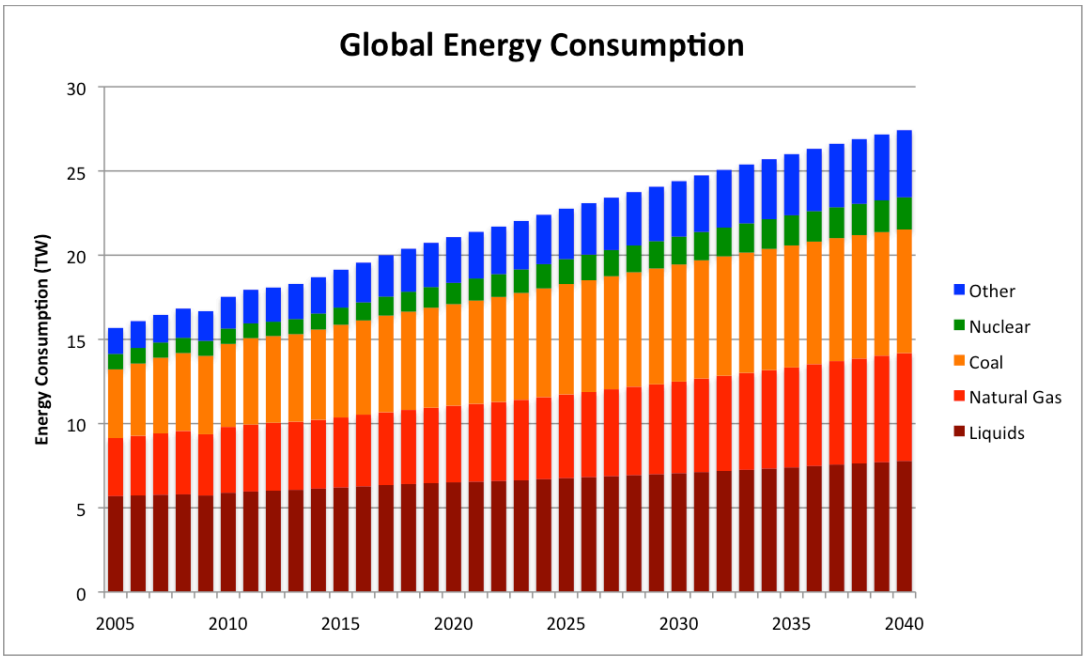


**Figure 1**. Global energy consumption data from 2005 to 2013 and projected global energy consumption up to 2040 (data taken from the USEIA International Energy Outlook 2013).

While effective, hydrocarbon combustion includes carbon emission, which is a significant source of atmospheric pollution. The global reliance on fossil fuels is so

severe that the USEIA projects an increase in carbon emissions of 46% from their direct combustion over the next 25 years. According to studies of long-term climate stabilization, carbon emissions are essentially cumulative for upwards of a thousand years.[2] Since carbon dioxide acts as a greenhouse gas by trapping ultraviolet radiation from the sun, high concentrations can have significant detrimental effects on the world climate.

The enormous scale of annual consumption of fossil fuels, which are non-renewable, also raises a question of sustainability. Projections based on 1998 fossil fuel usage estimates 40-80 years of known oil reserves available, 150 years of further estimated oil reserves available, less than 600 years of natural gas resources available, and between 1000-2000 years of coal resources available for consumption.[3] While these estimations indicate that fossil fuels could be used to power the world for hundreds of years, reliance on these fuel sources introduces two major problems. The first is the inevitability that the global non-renewable fuel reserves will eventually be exhausted. For example, despite increasing demand for fossil fuels, the global production of oil is expected to peak before 2025.[4] Secondly, harvesting fossil fuels from the earth is disruptive to both the environment and human health. This is evident through recent events such as the 2010 Gulf of Mexico oil spill and the 2010 West Virginia coalmine disaster. Although mining industries represent only 1% of the global workforce, mining accidents account for 8% of worldwide occupation-related deaths. Less obvious consequences of large-scale fossil fuel harvesting include significant lead, cadmium, sulfur, mercury, and nitrogen emissions into the environment. Air pollution is responsible for as many as 3 million premature deaths each year, which is approximately 5-6% of the

world mortality rate.[5] Efforts to slow or halt the consequences of fossil-fueled energy consumption have led to the research and development of new, clean energy sources.

**Generation of Fuels in Nature**

A significant inspiration for developing clean energy sources comes from studying the synthesis and consumption of energy in nature. Energy in its purest form is stored in chemical bonds. The cleavage of a chemical bond destabilizes the atoms involved, releasing energy that can be converted into mechanical work. Since the potential energy of a bond is not released until the bond is broken, the stored energy can be transported within high-energy molecules across cells or organisms. This is the basis of all natural energy production and consumption. For example, plants produce sugar molecules, which contain numerous carbon-carbon and carbon-oxygen bonds. Plants synthesize sugar through photosynthesis, utilizing radiation energy from the sun to split water and power the synthesis of simple building blocks for more complex energy-storing molecules.[6] Other organisms consume these molecules, using them as biological fuel and releasing them into the environment upon decomposition. Thus photosynthesis is vital to global energy cycle.

Photosynthesis is just one of many processes that use physical energy as a means to produce chemical energy. While photosynthesis is centered on photons causing the oxidative splitting of water into oxygen, hydrogen, and electrons for the purpose of catabolizing large sugar molecules, much simpler reactions that form chemical bonds exist. One of the simplest energy storing reaction is the reduction of two protons into molecular hydrogen. This bond stores an impressive 13.6 kJ per mole of hydrogen.[6] Due

to the simplicity of splitting hydrogen and its high energy output, a diverse group of organisms utilize this reaction to power biological processes. For example, many prokaryotes have been discovered that use hydrogenase enzymes to reductively produce hydrogen both photosynthetically and chemosynthetically, forming an energy-producing pathway that is independent of carbon and oxygen.[7] Hydrogenases are diverse in structure and are found in archea, prokaryotes, and even eukaryotes. There is a natural beauty in the efficiency and simplicity of hydrogen evolution as chemical energy, and it serves as an inspiration towards the development of effective artificial pathways of hydrogen production using physical energy.

**Hydrogen as a Renewable, Carbon-neutral Fuel Source**

In addition to functioning as a fuel in biological processes, hydrogen is combustible like hydrocarbon fuels. Since hydrogenases show that that producing hydrogen can be done through a variety of pathways, hydrogen has huge implications as a clean, renewable fuel. The potential energy stored in the chemical bond of hydrogen is well documented, and photosynthesis has already proven that high-energy chemical bonds can be synthesized using solar energy, an exceedingly abundant resource. Additionally, the combustion of hydrogen yields only water and energy, producing no carbon emissions that could contribute to atmospheric pollution and the greenhouse effect. But most importantly, hydrogen fuel solves some of the largest problems associated with current solar energy technology. The most efficient way to capture and store solar power is currently through the utilization of photovoltaic cells.[3] A major limitation associated with photovoltaic cells is their ability to maintain electron charge separation. Current methods to maintain charge

separation are inefficient, with a theoretical maximum conversion efficiency of 65%. Also, the dissipation of the charge over time makes storage and transportation of electricity from photovoltaic cells unfeasible, and they are expensive relative to the amount of energy they produce. The storage of energy produced from the sun is especially important because any given area is only able to utilize solar energy for a limited amount of time per day due to the earth's rotation. Thus solar fuels, such as hydrogen, are very necessary and widely recognized as the most effective product of the conversion of solar power into usable energy.

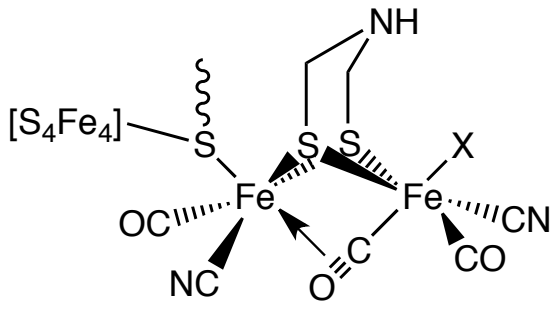


**Figure 2**. Active site of [FeFe]-hydrogenase consisting of a diiron-sulfur cluster.[8]

Using solar energy to form chemical bonds is difficult even for a molecule as simple as hydrogen. A molecule or system of molecules must be able to accomplish the redox reaction that synthesizes hydrogen from two protons and two electrons. The reaction is achieved naturally by very finely tuned enzymes such as [FeFe]-hydrogenase, which produce an effective kinetic and chemical environment to catalyze hydride formation and hydrogen production (Fig. 2). Even so, this reaction is highly susceptible to oxidative conditions, high potentials, and even high hydrogen concentrations. However, coordinative metal and organometallic complexes have been recognized to catalyze proton reduction.[8]

**Developing Metal Catalysts for Proton Reduction**

Following the structural elucidation of hydrogenases, there have been numerous efforts to synthesize structural mimics of these enzymes. These rationally designed catalysts for proton reduction fall under two main categories: ones utilizing a noble-metal center and ones containing abundant earth-metal ions instead. Noble-metal catalysts, such as platinum or palladium metal and related coordination compounds, are extremely effective at hydrogen production due to their ability to form hydride bonds and release hydrogen radicals that can combine to form hydrogen. However, these metals are extremely expensive and not viable for commercial use.[8] Abundant earth-metal catalysts, on the other hand, are much more inexpensive and commercially viable and thus more feasible as a global solution to the energy crisis. The variety of abundant earth-metals available for study combined with a continuously growing interest in alternative energy solutions has led to the discovery of numerous iron, cobalt, nickel, and molybdenum proton reducing electrocatalysts.[9]

While a diverse group of preliminary earth-abundant electrocatalysts for this process has already been discovered, optimizing these catalysts and elucidating the mechanisms behind catalysis has proven difficult. Developing an ideal transition-metal electrocatalyst for proton reduction requires that the complex be commercial viable, robust in its catalysis, and able to operate at a low overpotential. A complex's robustness refers to its stability as a catalyst. A robust catalyst is stable in air and aqueous environments and is able to achieve a high turnover number, which refers to the total number of times it can perform catalysis before it decomposes. It is optimal to have a very robust complex so that the catalytic cycle can be repeated the maximum number of

times without needing to replace the catalyst. The complex should also be able to be both oxidized and reduced so that it can complete a full redox cycle. If donating electrons to

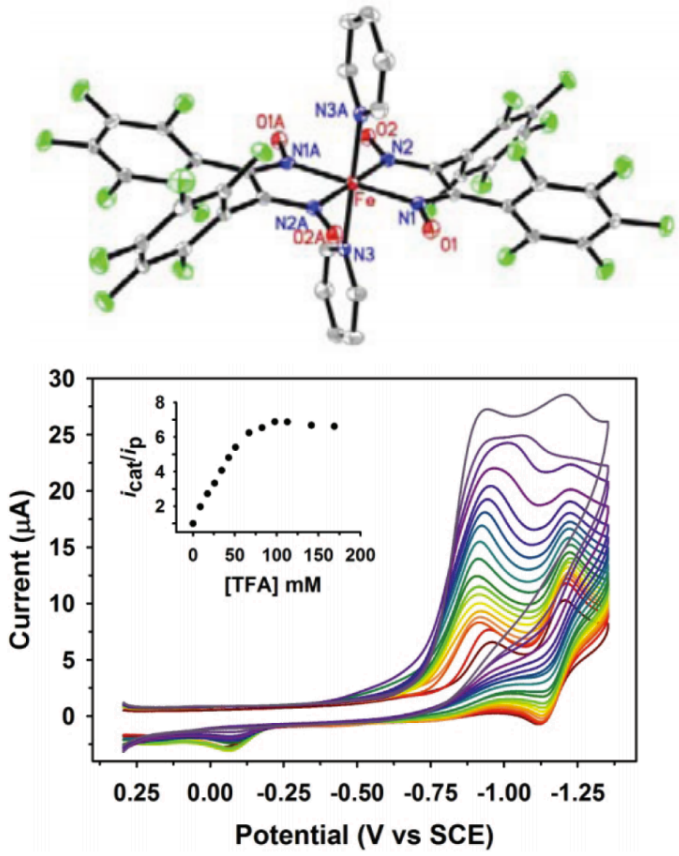


**Figure 3**. Representative cyclic voltammograms illustrating clear reduction waves upon increasing acid concentrations, which demonstrates catalytic activity by this fluorinated iron diglyoxime complex.[10]

hydrogen results in an irreversible oxidation of the complex, a redox cycle is not possible and the complex is useless as a catalyst. Cyclic voltammetry is used to determine whether or not catalytic reduction of protons is occurring. If a species is indeed an electrocatalyst, a growing reduction wave will be evident upon increased proton concentration (Fig. 3). The overpotential of a catalyzed redox reaction is the difference between the catalytic reduction potential and the thermodynamically ideal potential for reducing protons in the same conditions. It quantifies the activation energy barrier that the catalyst must

overcome to evolve hydrogen. Essentially, a high overpotential represents an activation energy barrier so high that the amount of energy needed to support catalysis yields the process too energy inefficient to be feasible. This is usually a result of thermodynamics, so the overpotential barrier can theoretically be lowered to the point where it is effectively non-existent, which is the case for many hydrogenases.[8] The use of an abundant metal as the metal center has already addressed the problem of commercial viability for these catalysts.

**Iron Complexes as Electrocatalysts for Proton Reduction**

Commercially viable earth-abundant metals used for proton reducing electrocatalyts are most frequently nickel, cobalt, iron, and molybdenum. Despite its prevalence in nature, there are very few examples of molecular iron electrocatalysts for hydrogen evolution in literature when compared to nickel and cobalt. Traditionally, nickel and cobalt complexes that successfully catalyze this reaction are both more active and efficient than iron complexes. Despite this, iron is the most attractive target metal for rational synthesis of homogeneous hydrogen generating catalysts because it is by far the most abundant transition metal, making it the cheapest and most feasible option for widespread use. Additionally, and likely for this exact reason, there is a clear natural precedence towards using iron for reducing protons.[11] Most iron electrocatalysts for hydrogen evolution are minimal structural mimics of [FeFe]-hydrogenase, containing the characteristic diiron-sulfur structure (Fig. 4). While they demonstrate modest electrocatalytic activity, their limited solubility in water represents a significant disadvantage to their feasibility as viable catalyst.[12] Catalysts containing a single iron center, such as Gray's fluorinated

diglyoxime-iron complex and Ott's iron carbonyl complex, operate at overpotentials as low as 300mV but still fail to solve the problem of water-solubility.[10,13] However, Berben's recent development of an iron-carbonyl clusters has demonstrated hydrogen evolution from buffer solutions up to pH = 9 (Fig. 5). The catalysis of proton reduction in these aqueous solutions occurs at an overpotential of 700-500mV depending on pH at

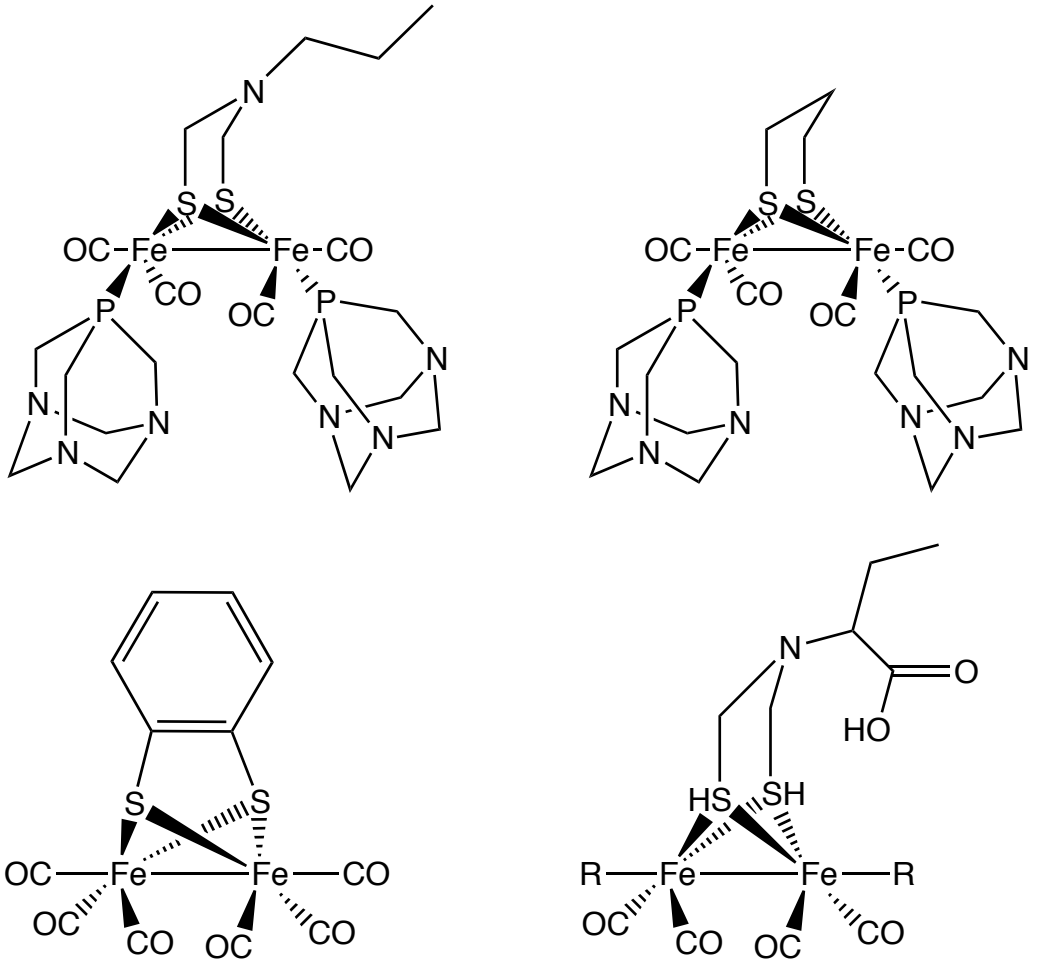


**Figure 4**. Diiron-sulfur [FeFe]-hydrogenase mimics that can electrocatalytically evolve hydrogen in organic solutions and mixed water-organic solutions. Water solubility is increased by the addition of the phosphaadamantane ligands.[12]

turnovers up to 34 over 150 minutes.[14] Despite these developments, a viable molecular iron electrocatalyst that operates at low overpotentials, high turnovers, and in aqueous solutions remains to be discovered.

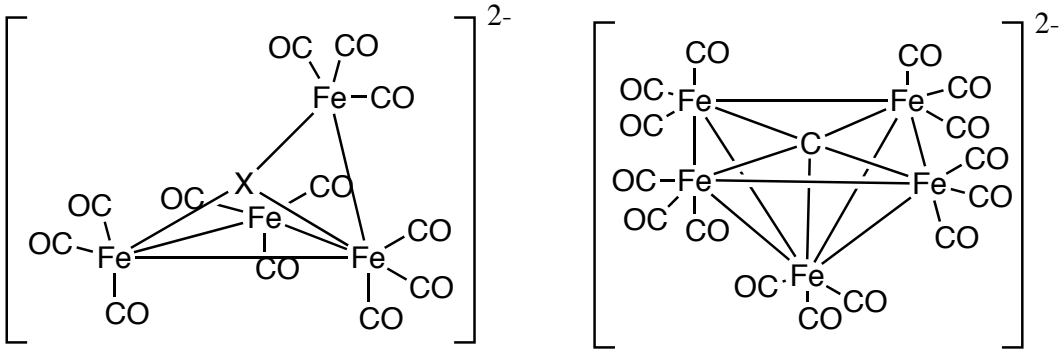


**Figure 5**. These iron carbonyl clusters are electrocatalytically active in aqueous buffer solutions and robust for hydrogen evolution up to 2.5 hours, but at fairly high overpotentials.[14]

**Molecular Photosystems for Generating Hydrogen**

The development of a viable iron electrocatalyst for proton reduction is necessary due to the role it plays in molecular photosystems for hydrogen evolution. These are single-molecule photocatalysts that produce hydrogen from a proton source and a sacrificial electron donor using energy from sunlight.[33,36] They operate very similarly to photosynthesis in that they combine two redox half-reactions to generate chemical fuel: an oxidation ($H_2O \rightarrow O_2$) and a reduction ($H^+ \rightarrow H_2$) (Fig. 6).[35] As in photosynthesis, photons excite electrons within a chromophore to a high potential. The electrons are injected from the chromophore's excited state directly into the conduction band of a semiconductor. They can then reduce the electrocatalyst during catalytic proton reduction, provided the overpotential for this reduction is low enough. The water oxidation catalyst serves as a reducing agent to the chromophore, replenishing the ground state and promoting overall forward electron transfer.

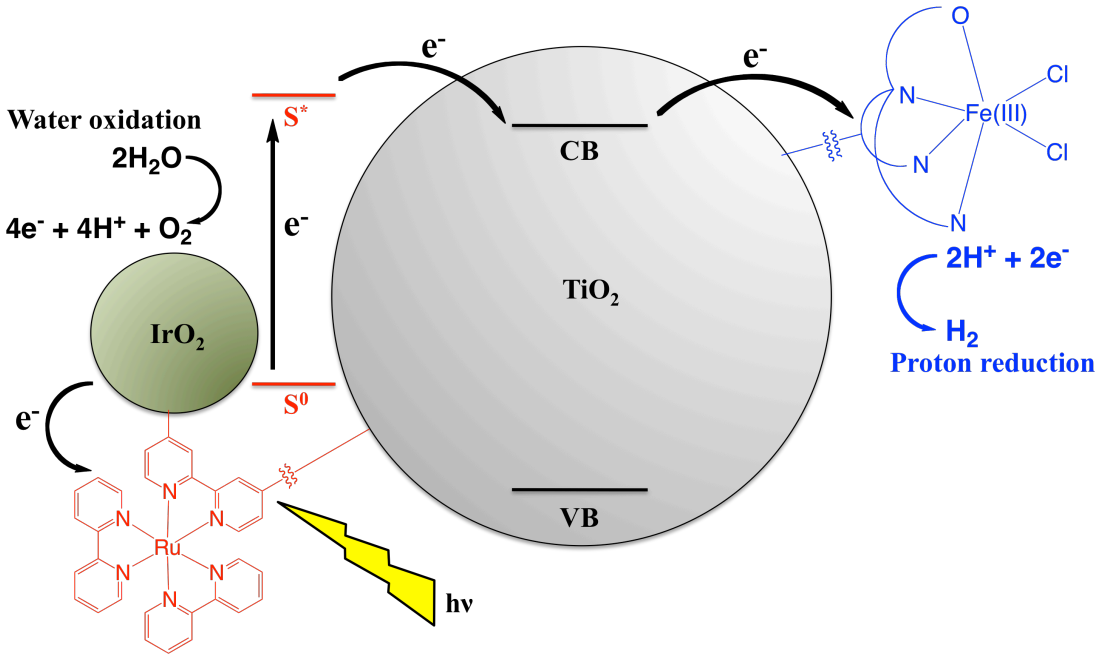


**Figure 6.** Model molecular photosystem for total water splitting. Mallouk et al. designed a molecular photosystem that utilizes a $TiO_2$ photoanode connected to a Pt wire that serves as both the cathode and catalyst for hydrogen production. This diagram shows $TiO_2$ nanoparticles as both the photoanode and photocathode for the redox chain and uses a theorized iron electrocatalyst for hydrogen production.[36]

Splitting water into hydrogen and oxygen using molecular photosystems is an elegant solution to generating clean fuel, but there are numerous unsolved problems with this approach to photocatalyzed hydrogen production. Oxidizing water requires the removal of four electrons, which is extremely difficult. Currently, the best catalysts for water oxidation are those utilizing noble-metal centers. Additionally, back electron transfer from the semiconductor to the chromophore competes with the forward electron transfer from the water oxidation catalyst. This back transfer results in a significant loss of efficiency. Electrons can also become trapped in band-gap states below the conduction band in the semiconductor.[37] In order to bypass these problems, the water oxidation half-reaction can be ignored in favor of using inexpensive sacrificial electron donors such as ascorbic acid. Photocatalytic generation of hydrogen has been reported at high rates in

aqueous solutions containing a chromophore, a cobalt-dithiolene catalyst, and ascorbic acid even without a conjunctive semiconductor.[36]

Although hydrogen can be generated photocatalytically without splitting water, a feasible molecular photosystem must operate in aqueous environments. This necessitates that the catalyst for proton reduction must be active in aqueous solutions. The catalyst must also be able to complete a high number of turnovers without decomposing so that the entire molecular photosystem can operate for extended periods of time. Since iron is the most abundant metal, it is the most logical target to use for photocatalytic hydrogen generation. It is therefore critical to develop robust, water-active iron electrocatalysts for proton reduction that can operate at low overpotentials so that they can be incorporated into molecular photosystems to generate clean, renewable hydrogen fuel from sunlight.

# Experimental

## Materials

All experiments were carried out using standard Schlenk air-free techniques under an Ar atmosphere unless otherwise indicated. All chemicals were purchased from Fischer Scientific and were used without further purification unless noted otherwise.

## Instrumentation

$^{1}H$ and $^{13}C$ spectra were recorded on a Varian Mercury 400VX spectrometer operating in the pulse Fourier transform mode. Chemical shifts are referenced to residual solvent. Coupling constants are reported in Hz. Elemental analysis was carried out by Atlantic Microlab, Norcross, GA 30071. All electrochemical experiments were performed under an atmosphere of Ar using a CH Instruments 620D potentiostat. Cyclic voltammograms were acquired using a standard three-electrode cell. Prior to each acquisition, the working electrode (glassy carbon) and the auxiliary electrode (platinum) were polished using 0.05 $\mu$m alumina powder paste on a cloth-covered polishing pad, followed by rinsing with water and acetonitrile. The reference was a SCE electrode unless otherwise noted. Ferrocene was used as an internal standard to correct for drifting of the reference electrode. Controlled potential coulometry was carried out in a sealed 500 mL cell using vitreous carbon working and counter electrodes and a Ag wire reference electrode. A CH Instruments 620D potentiostat combined with a CH Instruments 680 amp booster was used. Gas analysis for $H_2$ was performed using a Bruker Scion 436 gas chromatograph using Ar carrier gas and calibrated with 4 $H_2/CH_4$ gas mixtures of known composition.

## X-ray Diffractometry

Single crystals were mounted on glass fibers. All data for **2** were collected using graphite-monochromated Cu K$\alpha$ radiation ($\lambda$ = 1.54187 nm) on a Bruker-AXS three-circle diffractometer, equipped with a SMART Apex II CCD detector. The data were corrected for Lorentz effects and absorption using SADABS. The structure was solved using direct methods. Least squares refinement was carried out of $F^2$ for all reflections. The structure was refined using the SHELXTL software package.

## Syntheses

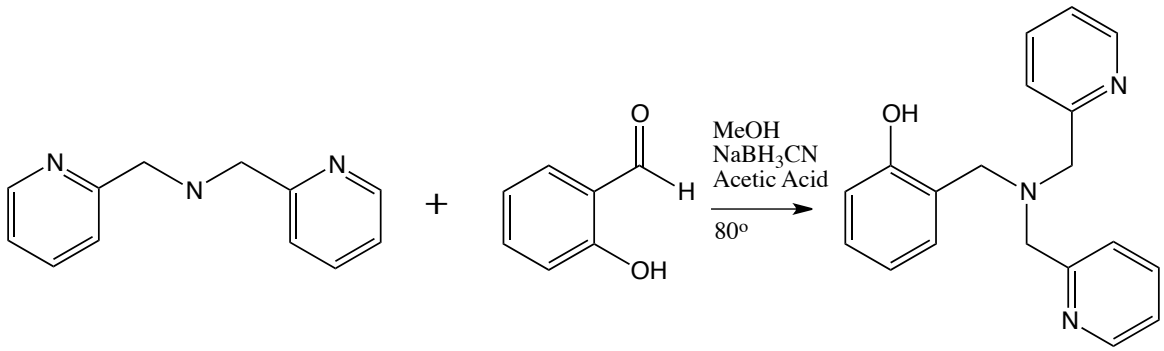


**Figure 7**. Scheme for synthesis of **1**.

N-(2-hydroxybenzyl)-N,N-bis(2-pyridylmethyl)amine (**1**) was synthesized using a modified literature procedure (Fig. 7).[15] Salicylaldehyde (1.00 mL, 10 mmol) in 50 mL of MeOH was degassed with Ar. To this, a degassed solution of bis(pyridin-2-ylmethyl)amine (1.80 mL, 10 mmol) in 10 mL of MeOH was added. 3 drops of glacial acetic acid were added followed by the dropwise addition of a degassed solution of sodium cyanoborohydride (0.31 g, 5 mmol) in 5 mL of MeOH. The resulting clear, yellow solution was refluxed for 1 hour and then stirred at room temperature overnight. 1 M HCl was added to the solution until it reached pH = 4 and turned from yellow to

amber. The solution was evaporated to near dryness and dissolved in 25 mL of saturated $Na_2CO_3$ solution and then extracted with chloroform (3 x 75 mL). The organic layer was dried with $Na_2SO_4$ and filtered through celite. The liquid was evaporated to dryness to yield an amber oil. **1** was purified through a silica gel column run sequentially in 99:1, then 19:1, then 9:1 DCM:MeOH. The purified **1** was collected at a yield of 59% (1.80 g, 5.88 mmol) as an amber oil. $^1$H NMR ($CDCl_3$): ∂ 8.49 (d, 2H), 7.57 (t, 2H), 7.29 (d, 2H), 7.10 (m, 3H), 7.00 (d, 1H), 6.84 (d, 1H), 6.70 (t, 1H), 3.81 (s, 4H), 3.73 (s, 2H) (Fig. 8).

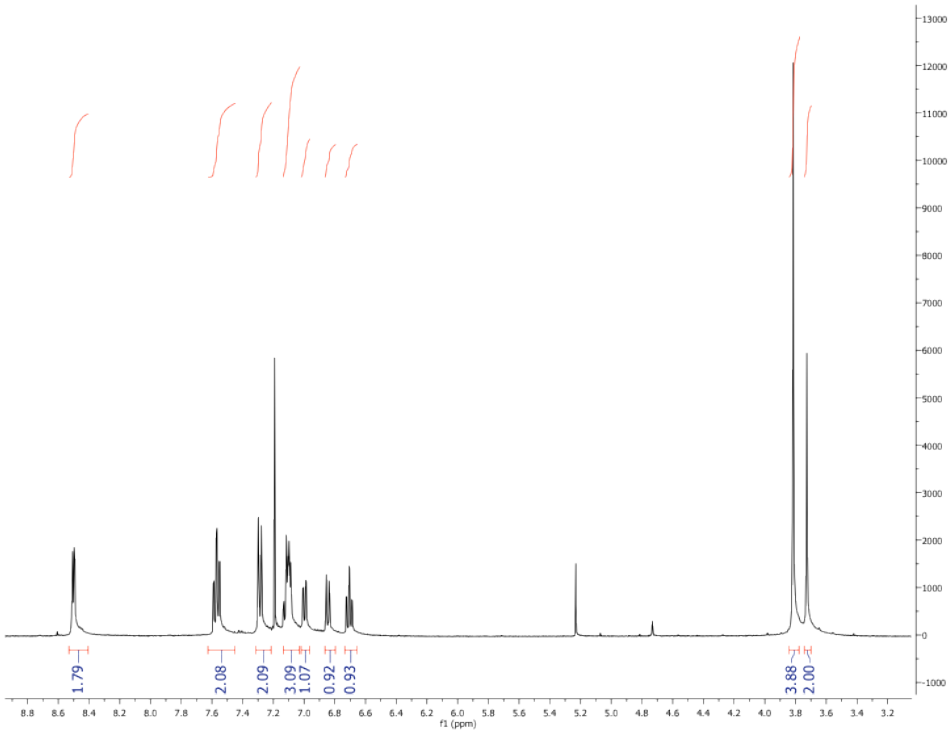


**Figure 8**. $^1$H NMR Spectrum of **1** with integrations in blue.

[$FeCl_2$(**1**)] (**2**) was synthesized using a modified literature procedure (Fig. 9).[15] **1** (1.798 g, 5.88 mmol) and triethylamine (0.475 g, 4.7 mmol) were dissolved in 10 mL of MeOH and degassed with Ar. $FeCl_3 \cdot 6H_2O$ (1.271 g, 4.7 mmol) was dissolved in 10 mL of MeOH and degassed with Ar. The two solutions were combined under air-free

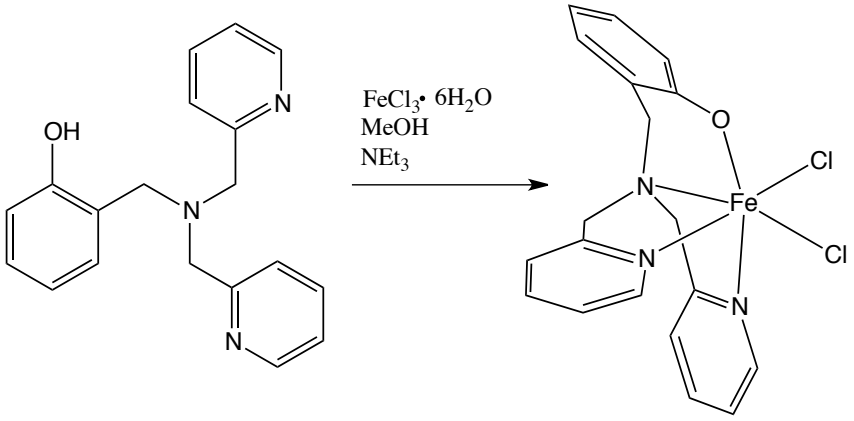


**Figure 9**. Scheme for synthesis of **2**.

conditions to yield a dark blue solution with a visible precipitate. The reaction was stirred at room temperature for 1 hour and filtered. The solid was washed with cold methanol (3 x 10 mL). A lustrous dark solid of **2** was collected with a 74% yield (1.502 g, 3.48 mmol). The product was crystallized by diffusion of hexanes into a concentrated solution of **2** in dichloromethane to yield blue feather crystals, which were collected via filtration. Crystals suitable for X-ray diffraction were grown by diffusion of diethyl ether into a concentrated solution of **2** in DCM (Fig. 10). Anal. Calcd. for **2** monohydrate $FeC_{19}H_{18}N_3Cl_2 \bullet H_2O$: C, 50.8; H, 4.49; N, 9.36%. Found: C, 50.66; H, 4.18; N, 9.13% (Fig. 11).

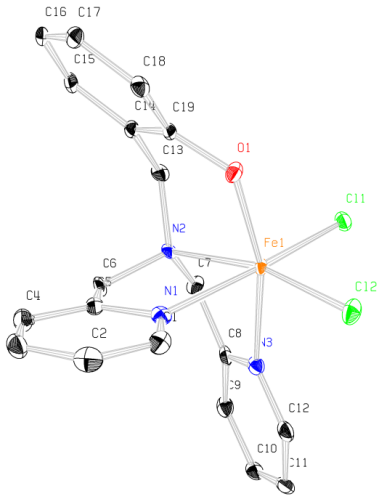


**Figure 10**. ORTEP diagram of **2**. Fe (orange), O (red), N (blue), C (black), and Cl (green). Hydrogen atoms have been omitted for clarity. Ellipsoids are at the 50% probability level.

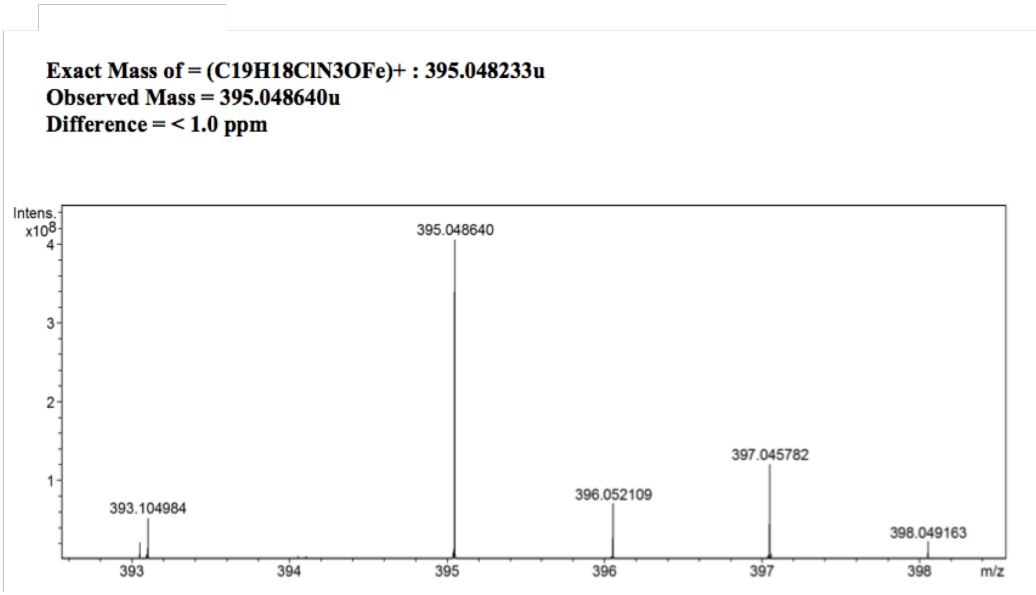


**Figure 11**. High-resolution mass spectrum of **2** in $H_2O$/MeOH. Analysis was completed through positive electrospray ionization on a Burker 12 Tesla APEX-Qe FTICR-MS with an Apollo II ion source. The molecular ion detected was charged due to the dissociation of a chlorine ion during testing. The expected molecular ions were observed with a difference of less than 1 ppm.

**Preparation of Buffer Solutions**

The buffer systems used for analysis of **2** were a citric acid/sodium phosphate buffer for pH = 3-7 and a monobasic/dibasic sodium phosphate buffer for pH = 8. The buffers were prepared in batches of 100 mL using 0.1 M citric acid, 0.2 M $Na_2HPO_4$, and 0.2 M $NaH_2PO_4$, all in de-ionized $H_2O$, in the following ratios:

**Table 1.** Preparation of various buffer solutions.

| *pH* | *Citric Acid (mL)* | *$Na_2HPO_4$ (mL)* | *$NaH_2PO_4$ (mL)* | *DI $H_2O$ (mL)* |
|---|---|---|---|---|
| 3 | 79.45 | 20.55 | 0 | 0 |
| 4 | 61.45 | 30.55 | 0 | 0 |
| 5 | 48.50 | 51.50 | 0 | 0 |
| 6 | 36.85 | 63.15 | 0 | 0 |
| 7 | 17.65 | 82.35 | 0 | 0 |
| 8 | 0 | 47.35 | 2.65 | 50 |

**Controlled Potential Coulometry**

Controlled-potential coulometry experiments (CPC) were conducted in a closed 500 mL four-neck roundbottom flask. For each pH level, 3.0-3.2 mg **2** (0.007-0.0074 mmol) was added to 50 mL aqueous buffer solution. The flask was capped with two vitreous carbon electrodes and a silver wire reference electrode, all submerged in the solution and separated by vycor frits. The flask was degassed using Ar for 20 minutes while the solution was stirred. Using a Hamilton gas syringe, 10 mL of Ar was removed from the flask and replaced with 10 mL $CH_4$ for reference. A cyclic voltammogram (CV) of the solution was then taken from 0 to -1.8 V to identify the proton reduction potential. A CPC was run at -1.2 V for 3600 seconds while the solution continued to stir. Upon completion of the experiment, a 10 mL sample of vapor from the flask was removed using a Hamilton gas syringe and injected into a GC. The ratio of $H_2$ to $CH_4$ in the

sample was compared to a calibration curve to determine the total volume of $H_2$ produced during the experiment (Fig. 12).

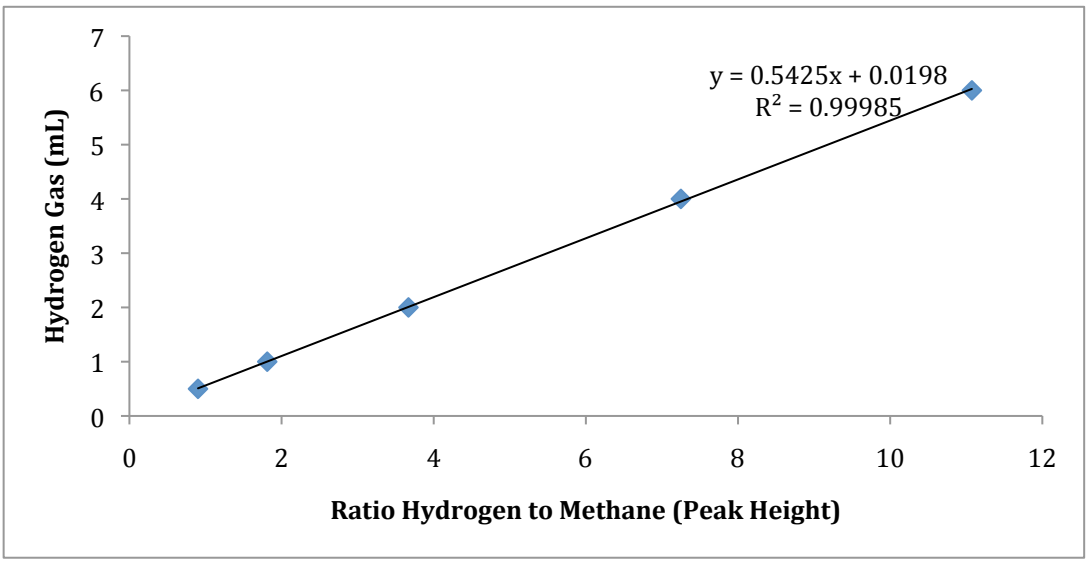


**Figure 12**. Calibration curve for $H_2$ to $CH_4$ ratios used for analysis of CPC experiments. The ratio of $H_2$ to $CH_4$ peak heights was plotted against the volume of $H_2$ in the sample ($R^2$ = 0.99985).

## Catalyst Concentration Dependence Study

A 25 mM stock solution of **2** was prepared by dissolving 0.077 g **2** crystals with $CH_3CN$ in a 10 mL volumetric flask. A 5 mL solution of 193 mg $TBAPF_6$ (0.1 M) in 1:1 $H_2O$:$CH_3CN$ was prepared in an electrochemical cell. 200 µL 1.1 M TFA (44 mM) was added to the cell, which was degassed with Ar. CVs were taken from 0.0 to -1.32 V at 200 mV/s without any catalyst, then after the addition of 40 µL, 60 µL, 80 µL, 100 µL, and 120 µL of the **2** stock solution. CVs were obtained using a glassy carbon working electrode, a Pt auxiliary, and an SCE reference electrode. The working and auxiliary electrodes were polished with 0.05 µm alumina powder paste prior to each acquisition.

**Scan Rate Dependence Study**

In an electrochemical cell, 1.0 mg **2** (2.32 μmol) was dissolved in 5 mL $CH_3CN$ with 0.1M $TBAPF_6$. CVs were taken at various scan rates ranging from 50 mV/s to 700 mV/s. CVs were obtained using a glassy carbon working electrode, a Pt auxiliary, and an SCE reference electrode. The working and auxiliary electrodes were polished with 0.05 μm alumina powder paste prior to each acquisition.

**pH Dependence Study**

In an electrochemical cell, 0.9-1.1 mg **2** (2.08-2.55 μmol) was dissolved in 5 mL aqueous buffer solution (pH = 3-8), with the buffer serving as the electrolyte. The solution was degassed with Ar to ensure an air-free environment. CVs were taken for pH = 3-5 from 0.0 to -1.4 V, for pH = 6 from 0.0 to -1.6 V, and for pH = 7-8 from 0.0 to -1.8 V at a scan rate of 100 mV/s. CVs were obtained using a glassy carbon working electrode, a Pt auxiliary, and an SCE reference electrode. The working and auxiliary electrodes were polished with 0.05 μm alumina powder paste prior to each acquisition.

**Determination of Overpotential**

The overpotential in acetonitrile was calculated according to literature procedure.[16] The overpotential in 1:1 $CH_3CN$: $H_2O$ was determined according to literature procedure using an open circuit potential measurement. The $E_{BH+}$ for TFA in this solvent mixture was determined to be -0.3991 V vs. SCE. The overpotential in this case is the difference between $E_{BH+}$ and $E_{p/2}$.[17]

## Results and Discussion

### Structure of Fe-NNNO Complex (2):

X-ray diffraction was used on dark blue plate crystals of **2** grown in diethyl ether:dicholoromethane slow diffusion experiments. The resulting crystal structure shows the Fe(III) metal ion bound to the pyridyl groups, the central amine, the phenol group, and two chlorides in a distorted octahedron (Fig. 13). The tetradentate-binding pattern of the ligand is encouraging because ligands with higher dentacity typically form more stable complexes with transition metals. Octahedral complexes typically have bond angles of 180° between axial positions in the coordination sphere, but the O-Fe-N and N-Fe-Cl bond angles were found to be 162.08°, 167.23°, and 166.99°, respectively. Additionally, the Fe-O bond length from the bound phenyl group is 1.826 Å, which is slightly shorter than other Fe(III) phenolate bonds reported in literature (1.905-18.480 Å).[18-20] Bond lengths (Å) and bond angles (°) for **2** are collected in Table 2, and selected X-ray crystallography data are collected in Table 3.

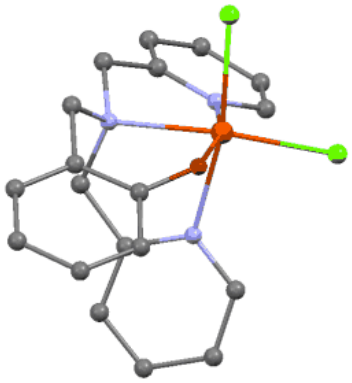

**Figure 13**. Crystal structure for **2**. Fe (orange), O (red), N (blue), C (black), and Cl (green). Hydrogen atoms have been omitted for clarity. The structure shows a distorted octahedron with $C_1$ symmetry.

**Table 2.** Bond lengths [Å] and angles [°] for **2**

| | |
|---|---|
| Fe(1)-O(1) | 1.896(2) |
| Fe(1)-N(3) | 2.179(3) |
| Fe(1)-N(1) | 2.198(3) |
| Fe(1)-N(2) | 2.250(3) |
| Fe(1)-Cl(2) | 2.2729(9) |
| Fe(1)-Cl(1) | 2.3425(9) |
| | |
| O(1)-Fe(1)-N(3) | 162.08(10) |
| O(1)-Fe(1)-N(1) | 85.67(10) |
| N(3)-Fe(1)-N(1) | 85.05(10) |
| O(1)-Fe(1)-N(2) | 88.94(9) |
| N(3)-Fe(1)-N(2) | 74.01(10) |
| N(1)-Fe(1)-N(2) | 76.61(10) |
| O(1)-Fe(1)-Cl(2) | 99.89(7) |
| N(3)-Fe(1)-Cl(2) | 96.13(8) |
| N(1)-Fe(1)-Cl(2) | 94.74(8) |
| N(2)-Fe(1)-Cl(2) | 167.23(7) |
| O(1)-Fe(1)-Cl(1) | 98.14(7) |
| N(3)-Fe(1)-Cl(1) | 87.82(7) |
| N(1)-Fe(1)-Cl(1) | 166.99(8) |
| N(2)-Fe(1)-Cl(1) | 90.97(7) |
| Cl(2)-Fe(1)-Cl(1) | 96.84(3) |
| C(19)-O(1)-Fe(1) | 131.0(2) |
| C(8)-N(3)-Fe(1) | 115.6(2) |

**Table 3.** Selected X-ray crystallography data for **2**.

| | |
|---|---|
| Empirical Formula | $C_{19}H_{18}Cl_2FeN_3O$ |
| fw (g/mol) | 431.11 |
| color/habit | dark blue plate |
| $T$ (K) | 100(2) |
| space group | $P2_1/n$ |
| $Z$ | 4 |
| $a$ (Å) | 14.9012(2) |
| $b$ (Å) | 7.05310(10) |
| $c$ (Å) | 17.5715(3) |
| $\alpha$ (deg) | 90 |
| $\beta$(deg) | 103.0850(10) |
| $\gamma$ (deg) | 90 |
| $V$ (Å$^3$) | 1798.81(5) |
| Final R-indices ($I$>2 $\sigma$) | 0.0408, 0.0996 |
| Final R-indices (all data) | 0.0487, 0.1062 |
| GOF | 1.027 |
| No. reflections measured | 17916 |
| No. of independent reflections | 3148 |
| $R_{int}$ | 0.0693 |

## Characterization of Fe-NNNO Complex (2) as an Electrocatalyst

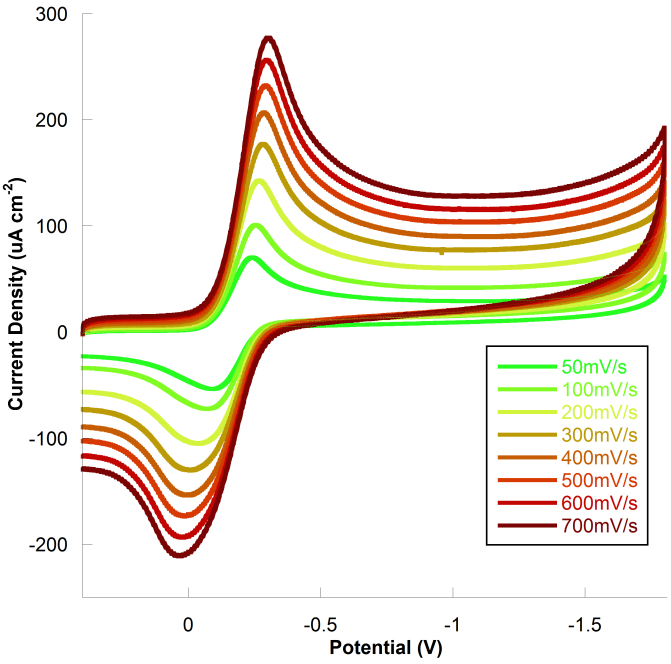


**Figure 14.** CVs of 1.0mg **2** in 5mL $CH_3CN$ with 0.1M $TBAPF_6$ from 0.2 to -1.8V with no acid added at various scan rates.

Cyclic voltammograms (CV) of **2** in acetonitrile ($CH_3CN$) showed a reversible Fe(III)/Fe(II) reduction at -0.28 V vs. SCE (Fig. 14). Upon addition of a proton source, trifluoroacetic acid (TFA), in acetonitrile, two

reductions occurred at -0.1 V and -1.17 V vs. SCE, respectively. Increasing TFA concentration caused the reduction peak at -1.17 V vs. SCE to increase in current accordingly, demonstrating a catalytic reduction of hydrogen at this potential (Fig. 15,

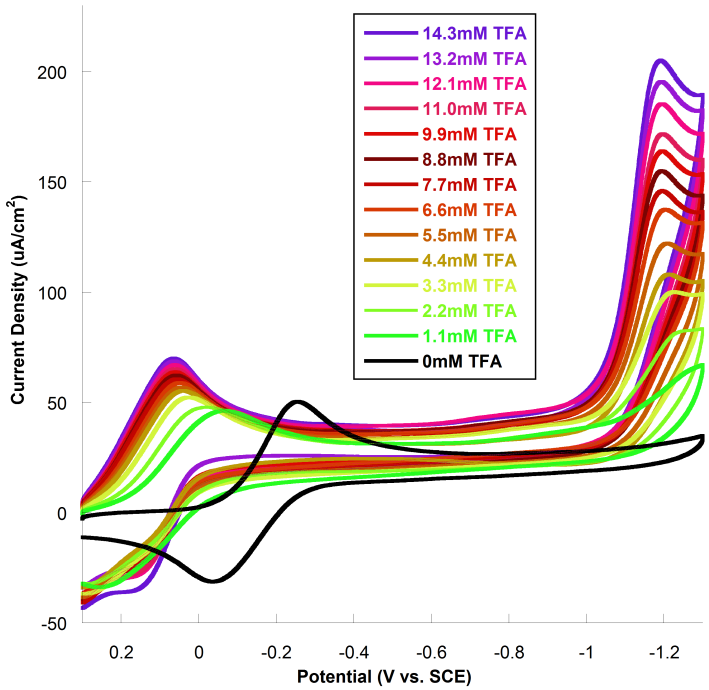


**Figure 15.** CVs of 0.3 mg **2** in 5 mL $CH_3CN$ with 0.1 M $TBAPF_6$ from 0 to -1.3 V at a scan rate of 50 mV/s without acid added (black) and upon the addition of increasing amounts of TFA. A catalytic reduction is visible at -1.17 V with an $i_c/i_p$ of 4.4.

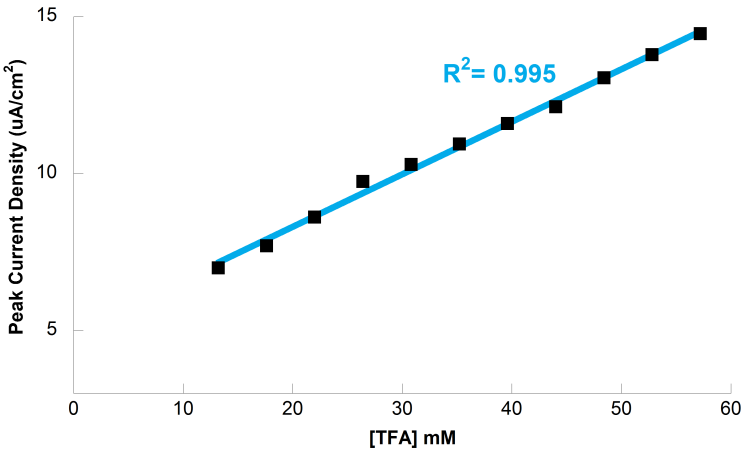


**Figure 16.** The peak current density vs. [TFA] corresponding to Fig. 15 was fit with a linear correlation exhibiting an $R^2$ value of 0.995. This indicates a second order reaction with respect to $H^+$.

colored traces). Graphing TFA concentration vs. peak current density of the catalytic reduction peak showed a linear relationship between proton concentration and catalytic activity, which corresponds to a second order reaction with respect to [$H^+$] (Fig. 16). In order to deduce the overall rate expression, the dependence of catalytic activity on catalyst concentration was determined using a catalyst concentration study (Fig. 17). The linear relationship between catalyst concentration and peak current density indicates a first order dependence of the reaction on catalyst concentration, which defines the rate expression as $rate = k[\mathbf{2}][H^+]^2$ (Fig. 18).

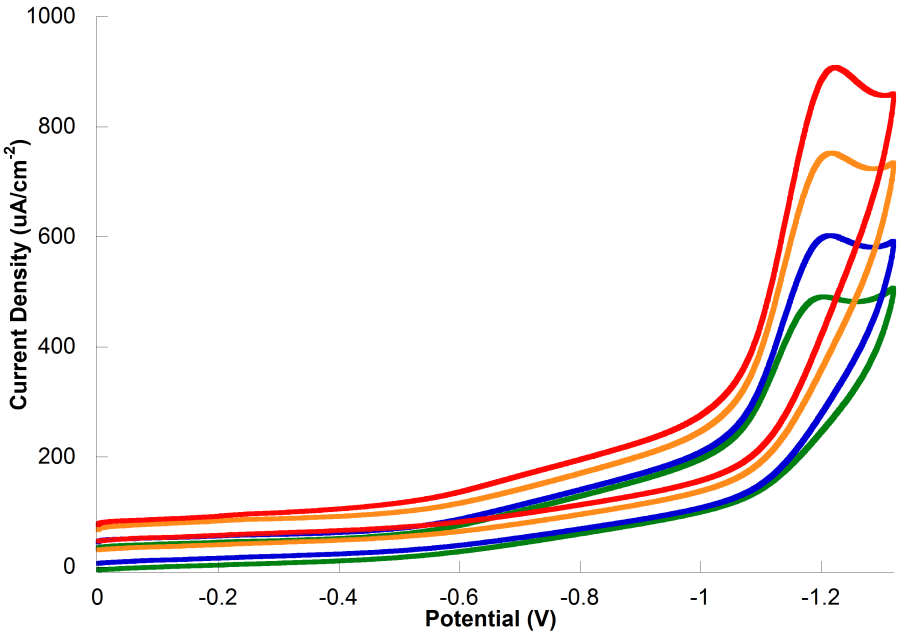


**Figure 17.** CVs of 5 mL 1:1 $H_2O$:$CH_3CN$ solution containing 44 mM TFA from 0.0 to -1.32 V at 200 mV/s with 0.2 mM (green), 0.3 mM (blue), 0.4 mM (orange), and 0.5 mM (red) **2** added in the presence of 0.1 M $TBAPF_6$.

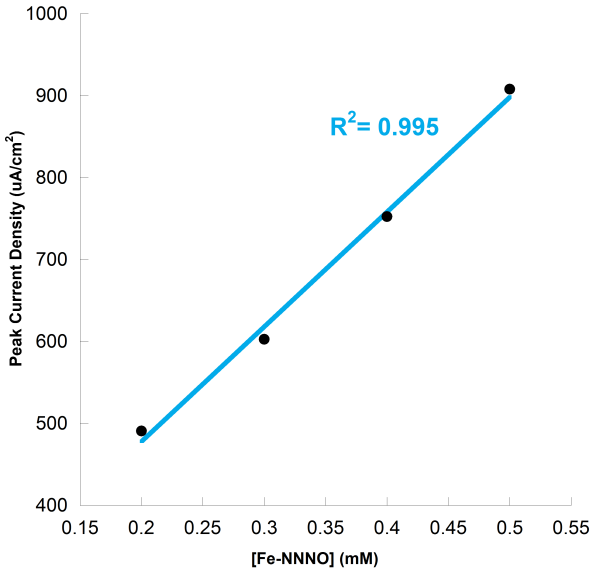


**Figure 18.** Peak Current Density vs. [**2**] Corresponding to Fig. 15. The linear correlation between PCD and catalyst concentration ($R^2$= 0.995) indicates a first order reaction with regards to **2**.

The cyclic voltammetry of **2** in the presence of TFA also provides valuable insight into the mechanism of catalytic hydrogen production. The redox couple for Fe(III)/Fe(II) shifts to a more cathodic potential in the presence of TFA. This indicates that a chemical transformation has occurred at the metal center, followed by an electrochemical reduction event. This chemical transformation is very likely the protonation of the phenolate, which forms the catalytic species. Since **2** becomes catalytically active only following this chemical transformation, the Fe(III) species can be considered a pre-catalyst. The initial reduction occurs at a slightly more cathodic potential as acid concentrations increase, indicating that a higher abundance of protons leads to easier protonation of the complex. The protonated and subsequently reduced species can then catalytically evolve hydrogen at -1.17 V vs. SCE. In order to confidently assert that catalytic activity is occurring in an electrochemical experiment, the peak current of the reduction event ($i_c$) in the presence of the substrate must be at least four times higher than the reduction potential of the catalyst without substrate present ($i_p$). The

voltammograms in Fig. 13 demonstrate that **2** generates $i_c/i_p$ values greater than four despite low proton concentrations, which confirms that the reduction event is indeed catalytic. In the return sweep, there is no oxidation event following the catalytic reduction event because the reduced species is catalytically regenerated, but the singly reduced Fe(II) species can be oxidized back to the pre-catalyst at 0.2 V.[23]

While the initial protonation and one-electron reduction of the Fe(III) center is clear, the overall mechanism of catalysis by **2** is difficult to deduce. One possible mechanism is a CEEC mechanism in which, following protonation and reduction of the pre-catalyst, the catalytic species undergos a second one-electron reduction. Rapid protonation of the electronegative Fe(I) metal ion would follow, and subsequent hydrogen evolution would be catalyzed by the proximity of the protons to each other and the availability of electrons at the doubly reduced metal center, yielding one molecule of hydrogen and recycling the original Fe(III) complex (Fig. 19). An alternative mechanism for catalytic proton reduction by **2** could be a CECE mechanism, once again initiated by the formation of the catalytic species by an initial protonation and one-electron reduction of Fe(III). In this case, a second chemical transformation could occur via direct protonation of the electron-rich Fe(II) metal site. A subsequent one-electron reduction would occur, followed by the evolution of hydrogen. It is important to note that it is extremely difficult to understand the exact mechanism of catalysis with the data collected so far. Additional experiments must be conducted with analogs of **2** to better understand the nature of its catalytic mechanism.

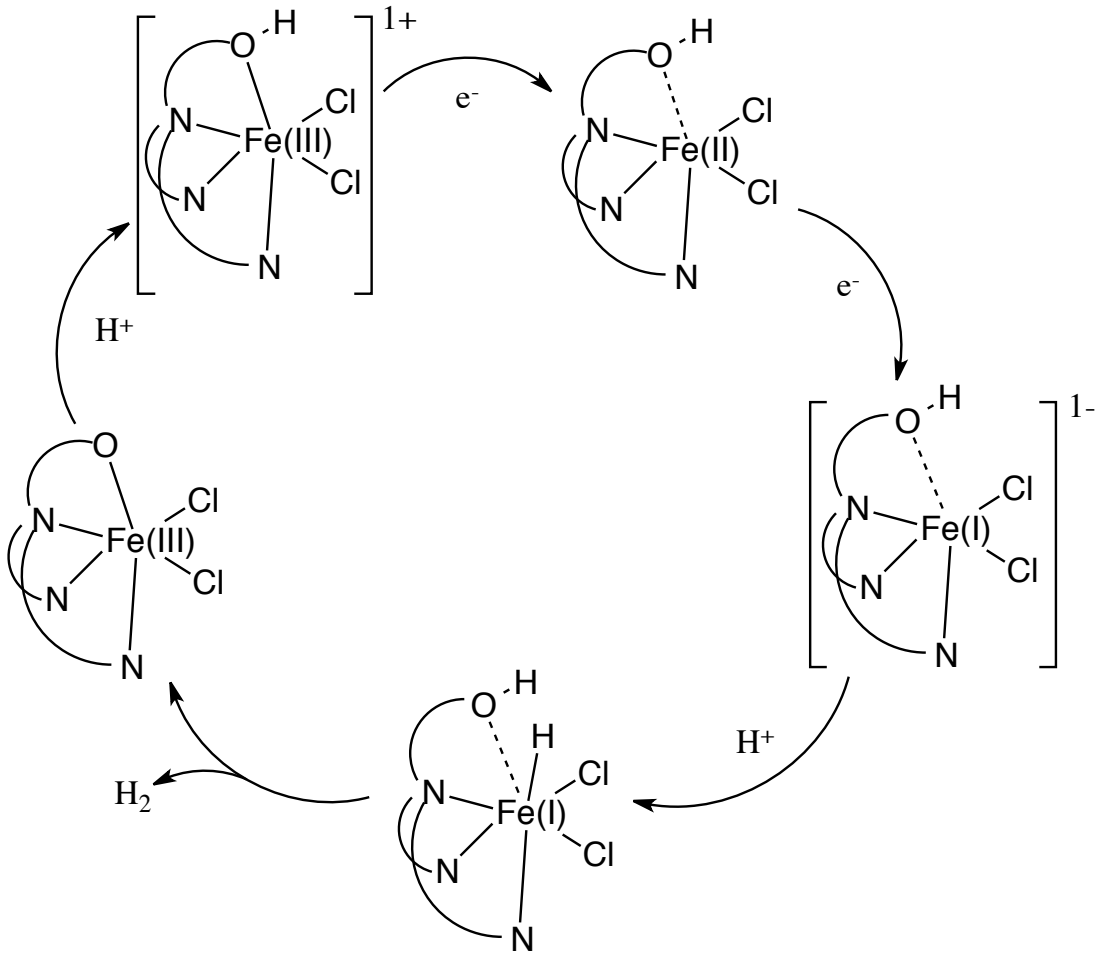


**Figure 19.** Proposed CEEC mechanism for catalytic proton reduction by **2**.

An ideal catalyst for proton reduction would be able to function with molecular photosystems in aqueous environments. It is therefore of great interest to characterize the behavior of potential catalysts in systems containing water. CV experiments were conducted to determine the catalytic efficacy of **2** in 1:1 water:acetonitrile solvent environments. Without a proton source present, the Fe(III)/Fe(II) reversible redox couple was identified at -0.4 V vs. SCE (Fig. 20). Upon addition of TFA to the system, an irreversible catalytic reduction event occurred at -1.32 V vs. SCE. Interestingly, the catalytic reduction current was much higher than observed in neat acetonitrile, yielding an $i_c/i_p$ of up to 15.6 after correction for background current.

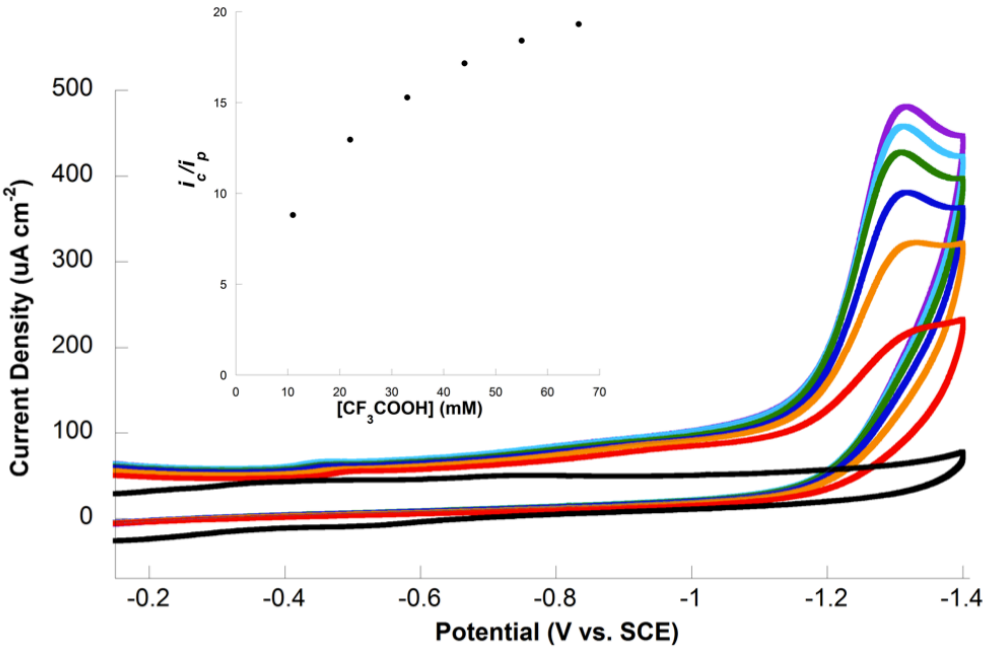


**Figure 20.** CVs of 0.4mg **2** in 5mL 1:1 ratio of $H_2O$:$CH_3CN$ with 0.1M $TBAPF_6$ from -0.1 to -1.4V at a scan rate of 200mV/s without acid added (black) and upon the addition of 11mM (red), 22mM (orange), 33mM (blue), 44mM (green), 55mM (light blue), and 66mM (purple) TFA.The Fe(III)/Fe(II) reduction peak without the addition of TFA occurs at -0.4 V with a current of 3.08 µA. Subtraction of baseline current and correction for dilution gives an $i_p$ of 1.76 µA. Inset: $i_c/i_p$ vs. [TFA] before corrections.

## Evaluating the Catalytic Activity of Fe-NNNO Complex (2)

A feasible earth-abundant transition metal complex for proton reduction would ideally satisfy four criteria defining its catalytic abilities: a low overpotential for the reaction, a high degree of activity, a high level of robustness, and the ability to function in aqueous environments. Experiments were conducted characterizing the catalytic abilities of **2** with regards to each of these criteria:

**Determining Overpotential**

As discussed earlier, overpotential for a hydrogen reducing electrocatalyst refers to the difference between the thermodynamically ideal potential for reduction of protons to hydrogen and the potential at which complex catalyzes this reduction. A low overpotential means that a catalyst can achieve the reaction with a lower energy requirement. Rational design of catalysts seeks to discover a system in which the overpotential is as close to zero as possible.

Determining the overpotential for **2** requires comparing the catalytic reduction potential of -1.17 V vs. SCE to the thermodynamic reduction of protons in the same solvent system. Literature values define the thermodynamic reduction of protons from TFA in acetonitrile occurs at -0.68 V vs. $Fc^{+}/Fc$, thus the overpotential for the catalytic reduction in acetonitrile was calculated to be 660 mV (Fig. 21).[17, 21-22] No literature

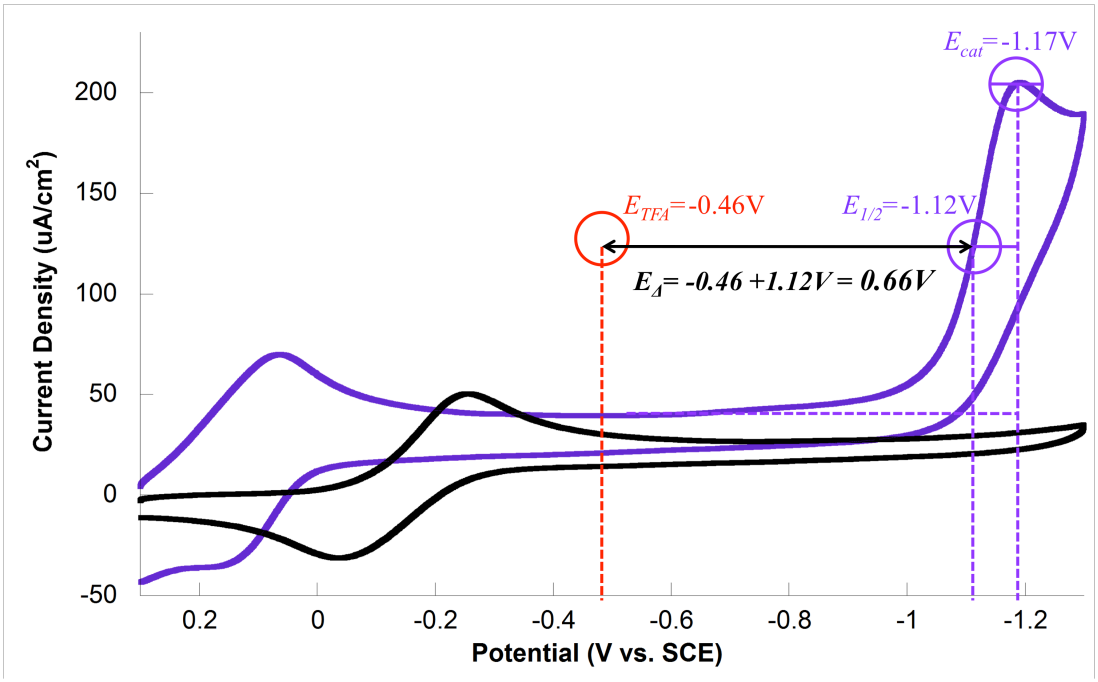


**Figure 21.** Determination of overpotential for **2** in acetonitrile. The thermodynamic reduction of TFA in acetonitrile occurs at -0.68 V vs. $Fc/Fc^{+}$, which corresponds to -0.46 V vs. SCE. This potential is compared with the potential at which the catalytic peak is at half current as described in literature to determine the overpotential.

values could be found detailing the thermodynamic reduction potential of protons from TFA in 1:1 water:acetonitrile, so this value was determined experimentally using open circuit potential techniques to be -0.393 V vs. SCE (Fig. 22). Comparison with the catalytic reduction potential in Fig. 20 shows that **2** operates at an overpotential of 800 mV in this solvent system. Overpotentials of 660-800 mV are comparable to other water-active efficient iron electrocatalysts; however, in organic solvent systems, overpotentials as low as 300 mV for iron complexes and below 250 mV for cobalt complexes have been reported.[10, 14, 24-25] Thus, while catalysts with significantly lower overpotentials exist, **2** operates at modest overpotentials even in aqueous environments.

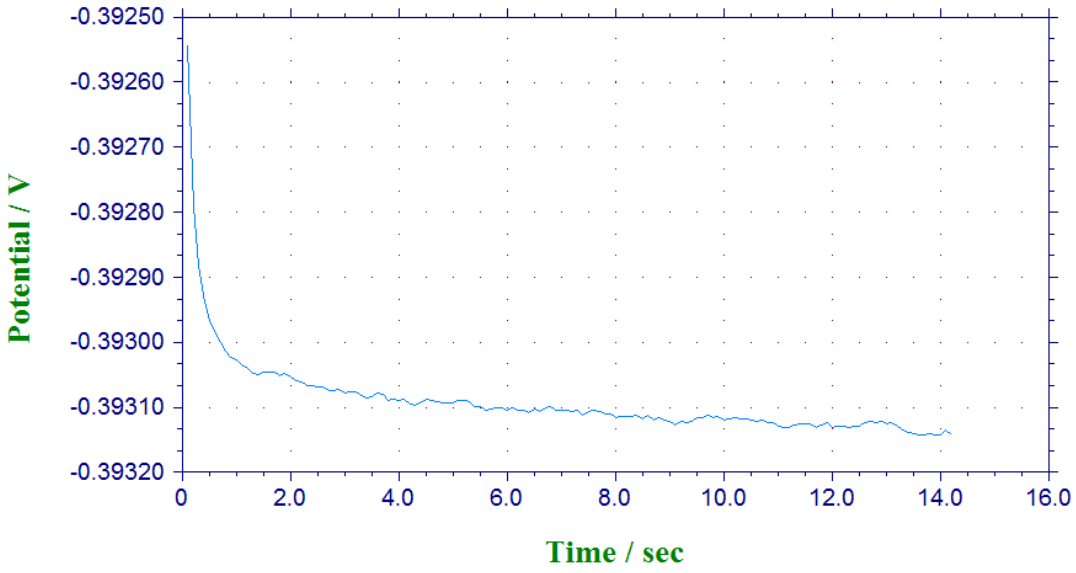


**Figure 22.** OCP experiment to determine the thermodynamic reduction of TFA in 1:1 water:acetonitrile. The reduction occurred at -0.3931 V vs. SCE.

Despite the operation of **2** at modest overpotentials, implementation of a hydrogen generating catalyst into a molecular photosystem will likely require much lower overpotentials. Fortunately, the ligand scaffold of **2**, especially the phenyl ring, is highly tuneable. This means that the introduction of electron-withdrawing groups, such as nitro

and halide groups, can affect the electronics of the reactive metal center. Electron-withdrawing groups will remove electron density from the metal ion, hypothetically allowing it to be reduced more easily. Facilitating reduction of the metal will theoretically result in a lower overpotential for catalytic proton reduction.

**Estimating Catalytic Rate**

The rate of catalytic activity for electrocatalysts can be estimated in a variety of different ways with varying degrees of error. Perhaps the simplest way to estimate catalytic activity is to use the $i_c/i_p$ value and the following equation, which describes pseudo-first-order catalytic systems,

$$\frac{i_c}{i_p} = \frac{n}{0.466}\sqrt{\frac{RTk_{obs}}{F\nu}} \quad (1)$$

where $n$ is the number of electrons in the each catalyzed reaction, $F$ is the Faraday constant, $\nu$ is the scan rate in V/s, $T$ is the temperature in K, and $R$ is the gas constant.[26-30] Solving for $k_{obs}$ gives the catalytic rate in $s^{-1}$. In the interest of comparing a wide array of electrocatalysts, Equation 1 has been extensively used to estimate catalytic reactions that are more complicated than pseudo-first-order EC mechanisms.[24] At high scan rates, the catalytic reaction at the electrode is not controlled by diffusion of substrate and catalyst at the electrode, so using a scan rate of 10 V/s provides the most accurate $i_c/i_p$ values (Fig. 23).

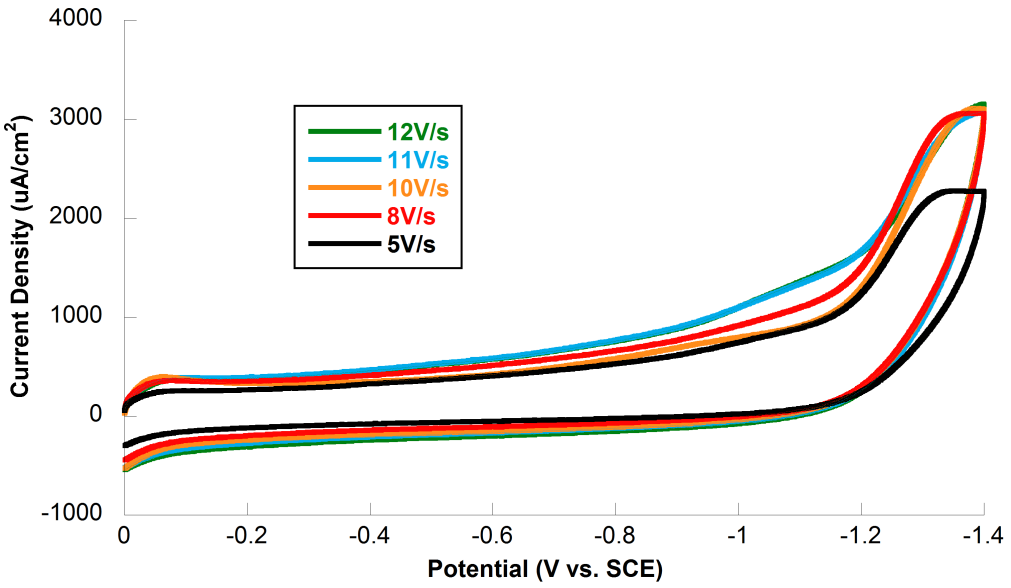


**Figure 23.** CVs of 1.0 mg **2** in 5 mL $CH_3CN$ with 17.6 mM TFA added at different scan rates in the presence of 0.1 M $TBAPF_6$. The $i_c$ plateau at -1.3 V becomes scan-rate independent at rates greater than 8V/s.

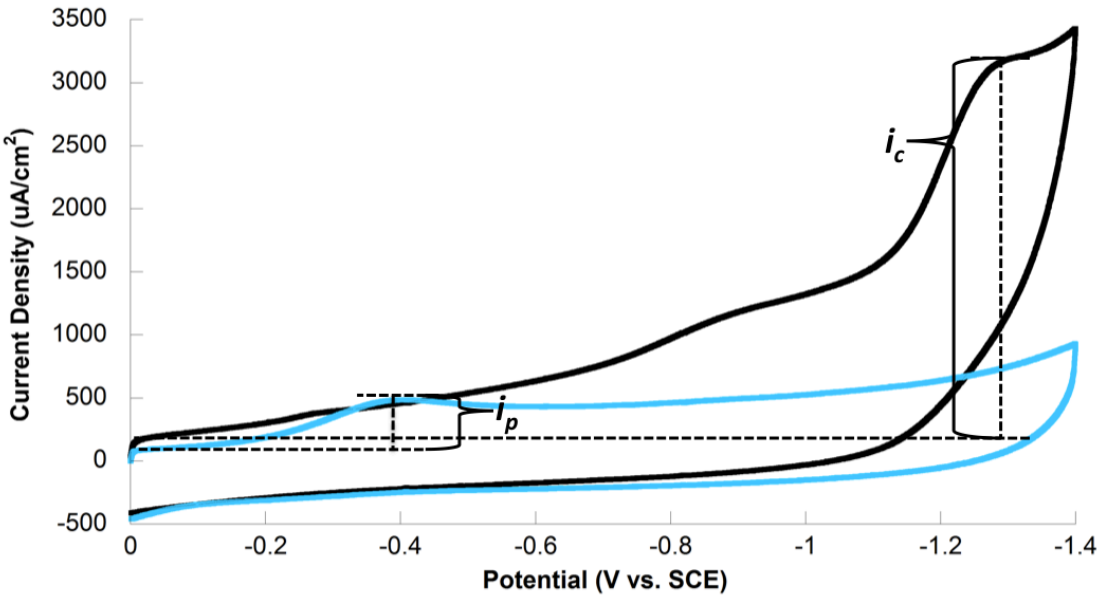


**Figure 24.** Determination of $i_c$ and $i_p$ data from cyclic voltammetry. CVs of 0.3 g **2** in 5 mL $CH_3CN$ before (blue) and after (black) the addition of 26.4 mM TFA in the presence of 0.1 M $TBAPF_6$. Scans were taken from 0.0V to -1.4 V at a rate of 10 V/s.

Fig. 24 illustrates how the values for $i_p$ and $i_c$ were determined experimentally. Using the experimental values, $k_{obs}$ was calculated in the following manner:

$i_p = 2.676 \times 10^{-5}\,\text{A}$
$i_c = 2.093 \times 10^{-4}\,\text{A}$

Correction of $i_p$ for dilution:[31]

$$i_p \times \frac{\text{vol}_i}{\text{vol}_f} \quad \rightarrow \quad (2.676 \times 10^{-5}) \times \frac{5.00mL}{5.12mL} = 2.613 \times 10^{-5}$$

Calculation of $i_c/i_p$:

$$\frac{2.093 \times 10^{-4}}{2.676 \times 10^{-5}} = 7.83$$

Calculation of $k_{obs}$:

$$k_{obs} = \left(\frac{i_c}{i_p} \times \frac{0.4463}{n}\right)^2 \left(\frac{F\upsilon}{RT}\right) \rightarrow \quad k_{obs} = \left(7.83 \times \frac{0.4463}{2}\right)^2 \left(\frac{96485 \times 10}{8.314 \times 293}\right) = 1209s^{-1}$$

A $k_{obs}$ of 1200s$^{-1}$ is the highest reported catalytic rate constant of an iron electrocatalyst for proton reduction.[10, 14] In 1:1 water:acetonitrile systems at 10V/s, the catalytic rate constant is even higher. Experimental values as high as 12.1 were obtained for $i_c/i_p$ after correction for background TFA reduction current (Fig. 25).

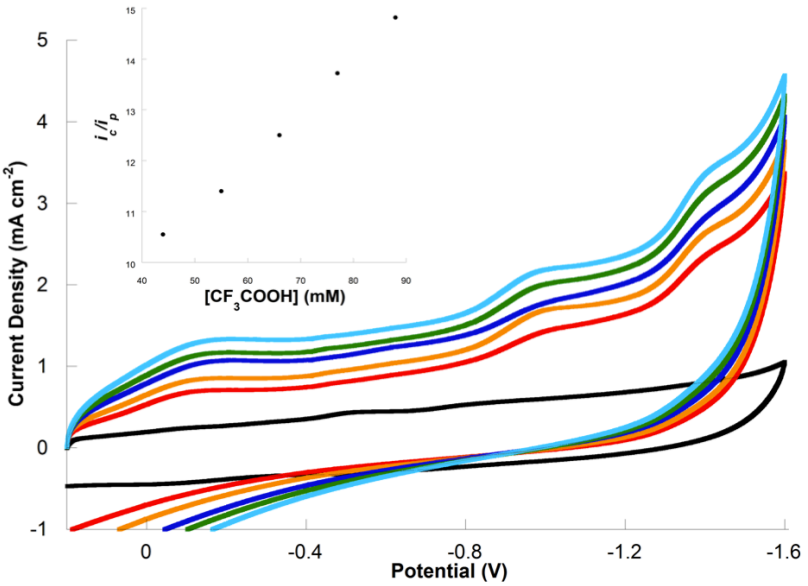


**Figure 25.** CVs of 0.3 mg **2** in 5 mL 1:1 ratio of $H_2O$:$CH_3CN$ with 0.1 M $TBAPF_6$ from 0.2 to -1.6 V at a scan rate of 10 V/s without acid added (black) and upon the addition of 44 mM (red), 55 mM (orange), 66 mM (blue), 77 mM (green), and 88 mM (light blue) TFA. The Fe(III)/Fe(II) reduction without the addition of TFA occurs at -0.51 V with a current of 30.4 µA. Subtraction of the baseline current and correction for dilution gives an $i_p$ of 16.5 µA. Inset: $i_c/i_p$ vs. [TFA] before baseline correction.

Using these values, $k_{obs}$ was calculated by the same method as before to be 3500s$^{-1}$. This establishes **2** not only as a highly active electrocatalyst for proton reduction, but also as the most active catalyst of its type discovered thus far.

A second method to estimate catalytic rate constants was employed in order to reinforce the validity of these experiments.[14,32] Equation 2 shows that the relationship between $i_c/i_p$ and $\nu^{-½}$ should be linear:

$$\frac{i_c}{i_p} = \frac{1}{\sqrt{\nu}}\left(\frac{2}{0.466}\right)\sqrt{\frac{RTk_{obs}}{F}} \qquad (2)$$

From this equation, the slope of $i_c/i_p$ vs. $\nu^{-½}$ can be used to calculate the observed $k_{obs}$ based on data collected over multiple scan rates rather than using just one. The $i_c/i_p$ of **2** was determined in neat acetonitrile and constant [H$^+$] at scan rates between 5 and 10 V/s, the speed at which the values for $i_c$ are essentially scan-rate independent. The $k_{obs}$ was calculated to be 1540s$^{-1}$ from the slope of the linear correlation between $i_c/i_p$ and $\nu^{-½}$ (Fig. 26).

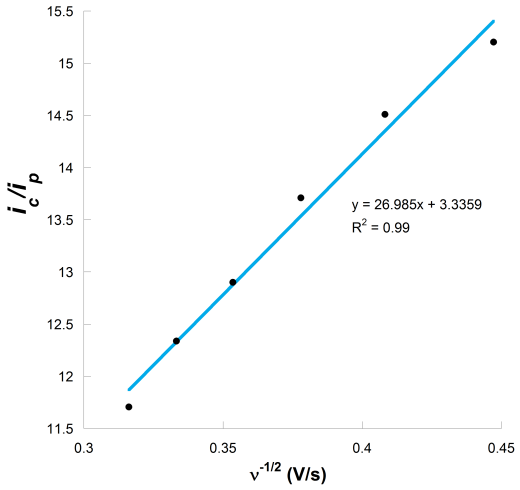


**Figure 26.** Linear correlation between $i_c/i_p$ and $\nu^{-1/2}$ for **2** at 5-10 V/s. CVs were taken in 5 mL $CH_3CN$ with 0.3 mg **2** in the presence of 0.1 M $TBAPF_6$ and 22 mM TFA. A slope of 26.985 was obtained with an $R^2$ value of 0.99.

This data suggests that the previous estimation was an underestimation of catalytic activity by **2**, but this is likely due to the fact that a slightly higher acid concentration was used for this study than the previous method. Regardless, the discrepancy between calculated catalytic rates in this experiment and the previous method is significant enough to merit further experiments to explore a value for experimental uncertainty.

### Confirming Catalysis in Aqueous Solutions

Although experiments in acetonitrile give insight into the catalytic mechanism, only iron catalysts that are active in aqueous solutions are feasible for incorporation into molecular photosystems. To this end, the catalytic activity of **2** in buffer systems of differing pH was explored.

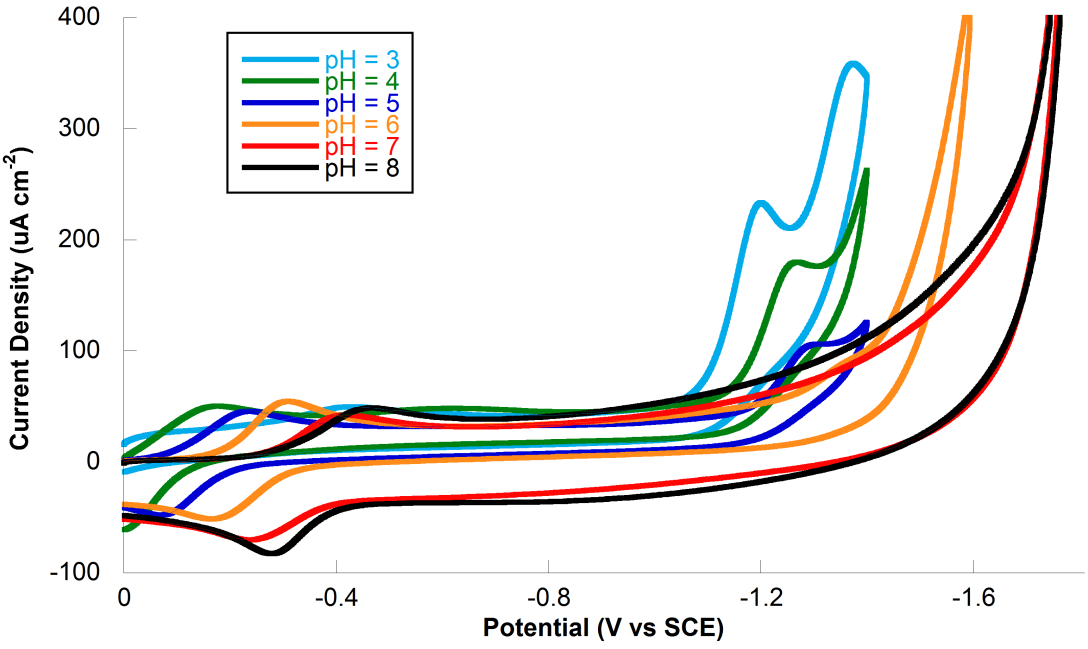


**Figure 27.** CVs of 1.0 mg **2** in 5 mL aqueous buffer solutions (pH = 3-7 citrate-phosphate buffer, pH = 8 phosphate buffer) at 100 mV/s from 0.0 to -1.4 V at pH= 3-5, from 0.0 to -1.6 V at pH=6, and from 0.0 to -1.8 V at pH= 7-8. Electrocatalytic activity is evident from pH= 3-6.

CVs were taken of **2** in six different citrate-phosphate buffer systems, showing catalytic reduction waves in pH = 3-6 (Fig. 27). These results confirm that the catalyst is indeed water stable and active in purely aqueous environments, a necessary criterion for inclusion in a molecular photocatalyst for hydrogen production. Fig. 27 illustrates that both the Fe(III)/Fe(II) reduction potential and the catalytic reduction potential vary as a function of pH. Pourbaix diagrams, which explore this relationship between pH and reduction potential, show that Fe(III)/Fe(II) reduction event varies by 77 mV per pH unit while the catalytic reduction event varies by 59 mV per pH unit (Fig. 28, 29).

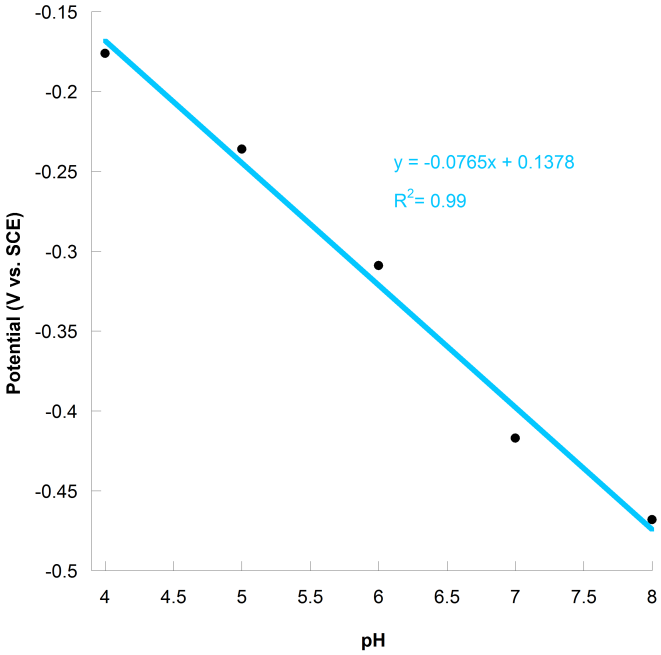


**Figure 28.** Pourbaix diagram of Fe(III)/Fe(II) reduction of **2**. The slope of the linear fit is -0.0765 V per pH unit with an $R^2$ value of 0.99.

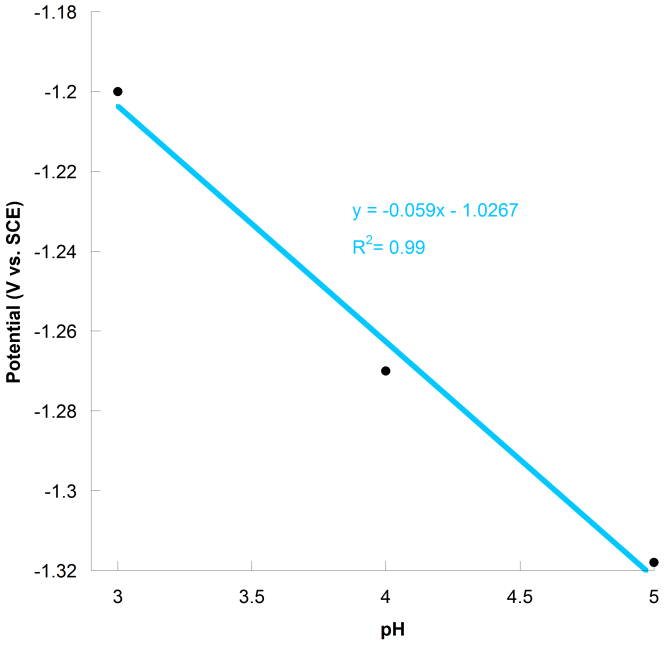


**Figure 29.** Pourbaix diagram for the catalytic reduction of hydrogen by **2**. The slope of the linear fit is -0.059 V per pH unit with an $R^2$ value of 0.99.

Analysis of the Nernst equation, which is the fundamental

relationship between chemical and electrical energy, shows that the amount of electrical energy change is:[28]

$$-\frac{2.303RT}{nF}\log Q$$

where $n$ is the number of electrons involved in the process, $F$ is Faraday's constant, $R$ is the gas constant, $T$ is the temperature in K, and $Q$ is the reaction quotient.

Simplifying the equation shows that:

$$-\frac{0.0592V}{n}\log Q$$

For one change in pH unit, $Q$ is 10 and log $Q$ is one, leaving:

$$-\frac{0.059V}{n}$$

This shows that a one-electron reduction event would correspond to a 59 mV change per pH unit, while a two-electron reduction event would correspond to a 29 mV change per pH unit. Thus both the Fe(III)/Fe(II) reduction event and catalytic reduction event are confirmed by the Pourbaix diagrams to be one-electron events with reasonable confidence. This information is extremely helpful in determining the mechanism of catalysis by **2**.

**Assessing Robustness**

Robustness is a relative term referring to a catalyst's stability in air and aqueous environments as well as its ability to achieve a high turnover number. Controlled potential coulometry (CPC), which involves applying a continuous potential at the catalytic voltage to a solution containing the catalyst and the substrate in a closed system, gives some insight into the robustness of a catalyst. A robust catalyst will consume

current continuously over a long period of time without decomposing. Additionally, analysis of the gases within the reaction vessel following CPC experiments can prove that the current consumed during the duration was indeed used to generate hydrogen gas. The total amount of charge consumed can then be compared to the amount of hydrogen evolved in order to estimate the efficiency of the catalyst. The ratio of product produced to charge consumed is known as the Faradaic yield.

A CPC experiment was conducted in pH = 5 citrate-phosphate buffer solution in order to determine the Faradaic efficiency and robustness of **2**. A potential of -1.2 V was applied over 60 minutes to the catalyst solution in a closed system containing 10 mL of methane gas as an internal standard. The catalyst demonstrated a constant consumption of current over the entire span of the experiment up to a total charge of 31.4 C (Fig. 30).

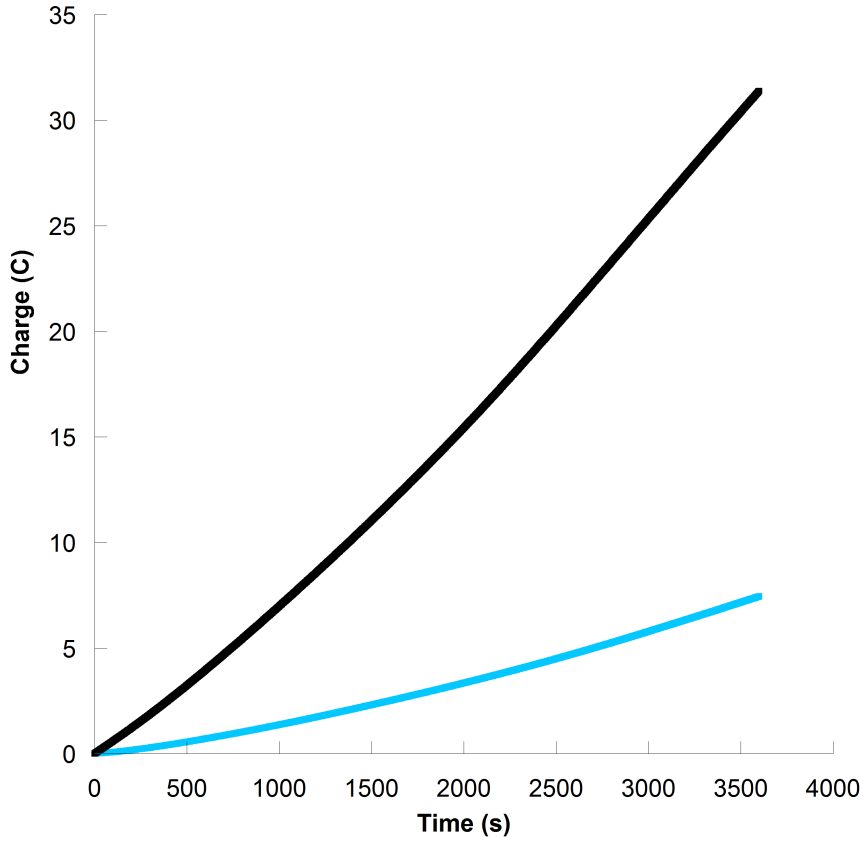


**Figure 30.** CPC with 3.0 mg **2** in 50 mL pH = 5 (black) buffer solution (0.139 mM) versus a control containing no **2** (light blue) at -1.2 V for 3600 seconds.

A sample of the gases present in the closed reaction system was analyzed using GC-TCD and compared to the calibration curve to determine the amount of hydrogen gas evolved during the experiment:

| | | | |
|---|---|---|---|
| $H_2$ – | height = 276812.1<br>area = 16425.6<br>time = 0.75 min | $CH_4$ – | height = 42197.8<br>area = 9852.5<br>time = 3.42 min |

$$y = 0.5425\left(\frac{276812.1}{42197.8}\right) + 0.0198 = 3.5785 \text{ mL } H_2$$

$$\frac{3.5785 \times 10^{-3} \text{ L}}{22.4 \text{ L}} H_2 = 1.598 \times 10^{-4} \text{ mol } H_2$$

Assuming 100% Faradaic yield, 31.4 C of charge would equate to $1.628 \times 10^{-4}$ mol $H_2$:

$$31.4 \text{ C}\left(\frac{1 \text{ e}}{1.6022 \times 10^{-19} \text{ C}}\right)\left(\frac{1 \text{ mol e}}{6.02 \times 10^{23} \text{ e}}\right)\left(\frac{1 \text{ mol } H_2}{2 \text{ e}}\right) = 1.628 \times 10^{-4} \text{ mol } H_2$$

Thus, from the following ratio, an experimental Faradaic yield of 98% was calculated:

$$\frac{1.598 \times 10^{-4} \text{ mol } H_2}{1.628 \times 10^{-4} \text{ mol } H_2} \times 100\% = 98\% \text{ Faradaic yield}$$

The total turnover number (TON), which is the total number of times the catalyst induced the reaction in the time allowed, was calculated as a simple ratio of moles hydrogen evolved over moles catalyst present:

$$\frac{1.598 \times 10^{-4} \text{ mol } H_2}{6.959 \times 10^{-6} \text{ mol } \mathbf{2}} = 23.0$$

This TON is likely a significant underestimate of the actual turnover ability associated with **2** due to the very limited surface area of the electrode available through which the necessary potential could be applied to the complex, inducing catalysis. Nevertheless, 23.0 turnovers over the course of one hour compares very favorably to Berben's aqueous iron cluster catalyst, which showed 34 turnovers over 2.5 hours.[14] While this is true,

comparing the TON of two catalysts is not a reliable method of analysis due to the inability to keep reaction conditions, especially exposed electrode surface area, constant between experiments.

The constant build-up of charge over the entire CPC experiment is a testament of the robustness of **2**. As shown in Fig. 24, the catalyst was active even in highly acidic environments where pH = 3. These observations support the notion of **2** as a feasible proton reducing electrocatalyst due to its water-stability, robustness, and resistance to harshly acidic environments. Additionally, the high number of turnovers achieved after just one hour of continuous catalysis shows that **2** is a highly active electrocatalyst, especially for an iron complex. Even more promising is the catalysts high ability to use the available electrons towards reducing protons, for a Faradaic yield of 98% is very nearly approaching unity.

Admittedly, a major concern drawn from the citrate-phosphate buffer experiments is the inability for **2** to catalyze hydrogen generation in neutral and alkaline environments. A complex that can catalyze proton reduction over a more diverse pH range is advantageous for incorporation in a total water splitting molecular photosystem because ideally these systems would be functional in commercial water sources. Thus **2** would be better suited for use in a molecular photosystem that utilizes a sacrificial electron donor such as ascorbic acid, which would result in more acidic solutions.

**Control Experiments**

A variety of experiments were performed to make sure that the metal complex was indeed acting as a catalyst for proton reduction. Direct reduction of TFA at the working

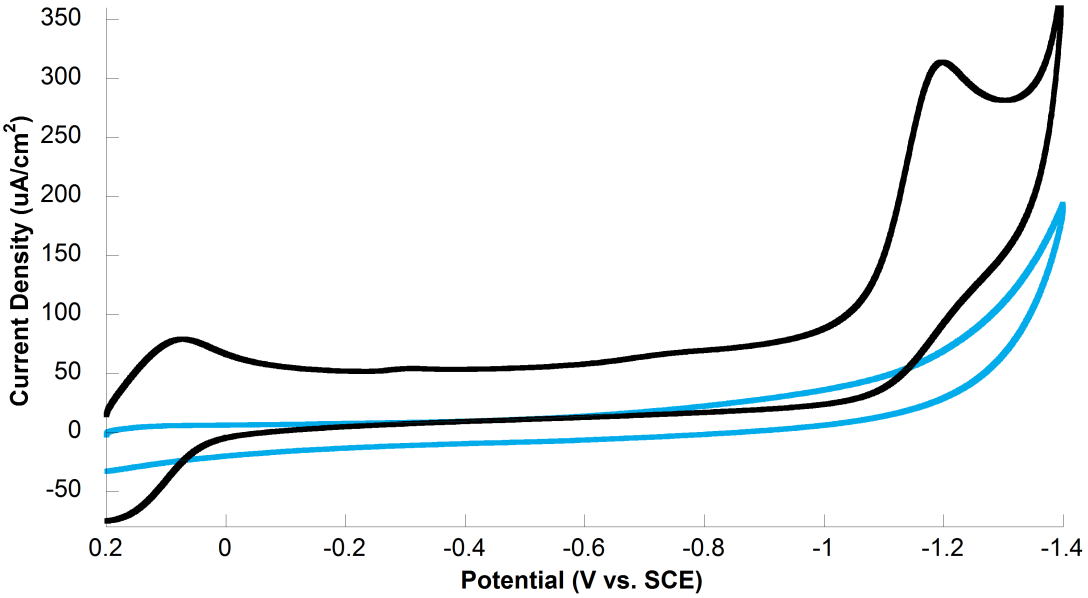


**Figure 31.** CVs of 22 mM TFA in $CH_3CN$ with 0.1 M $TBAPF_6$ prior to (light blue) and after (black) the addition of 0.5 mM **2** from 0 to -1.4 V at a scan rate of 200 mV/s. A reduction peak corresponding to the catalytic reduction of hydrogen is visible at -1.2 V only upon addition of **2**.

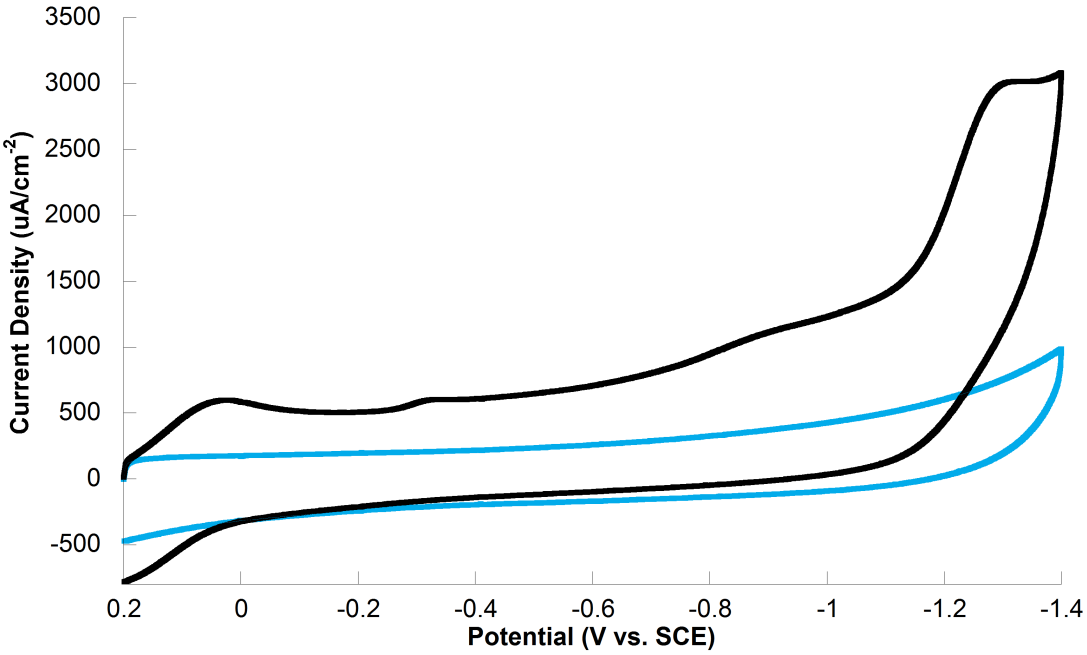


**Figure 32.** CVs of 22 mM TFA in $CH_3CN$ with 0.1 M $TBAPF_6$ prior to (light blue) and after (black) the addition of 0.5 mM **2** from 0 to -1.4 V at a scan rate of 10 V/s. A reduction peak corresponding to the catalytic reduction of hydrogen is visible at -1.25 V only upon addition of **2**.

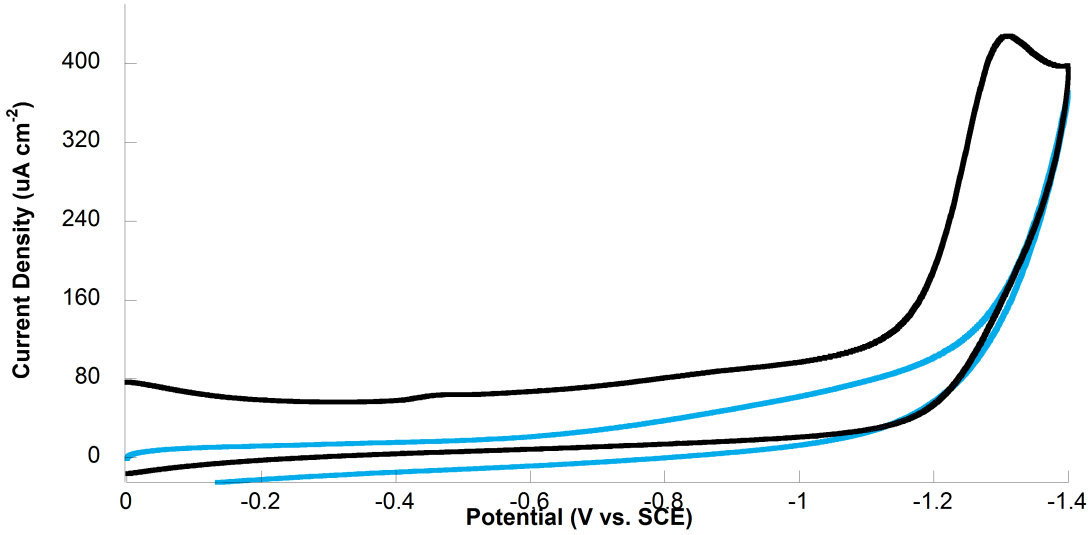


**Figure 33.** CVs of 44 mM TFA in 1:1 $H_2O$:$CH_3CN$ with 0.1 M $TBAPF_6$ prior to (light blue) and after (black) the addition of 0.4 mg **2** from 0 to -1.4 V at a scan rate of 200 mV/s. A reduction peak corresponding to the catalytic reduction of hydrogen is visible at -1.3 V only upon addition of **2**. Direct reduction of TFA in this solution was found to account for 18% of the total current at -1.3 V.

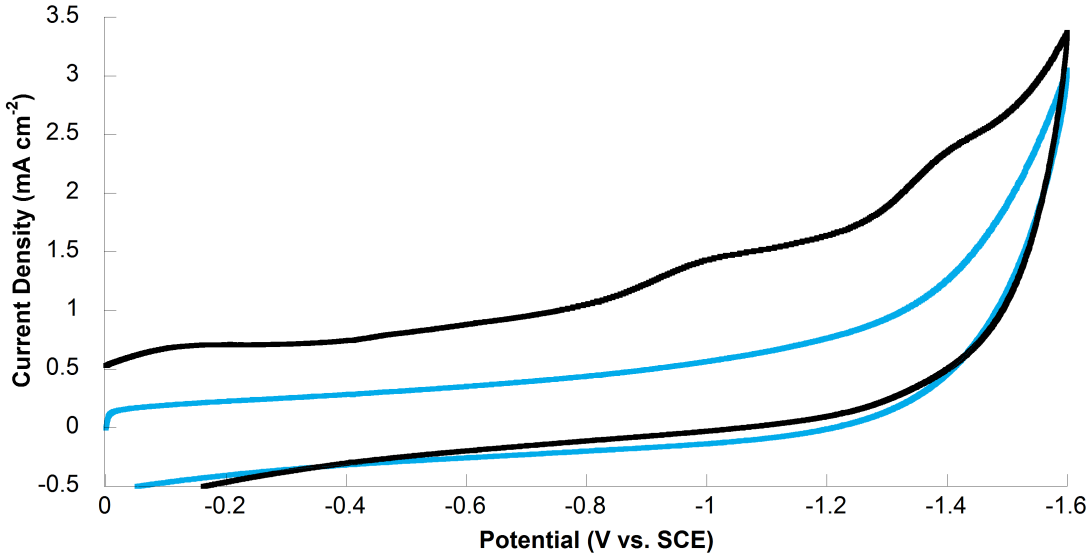


**Figure 34.** CVs of 44 mM TFA in $CH_3CN$ with 0.1 M $TBAPF_6$ prior to (light blue) and after (black) the addition of 0.3 mg **2** from 0 to -1.6 V at a scan rate of 10 V/s. A reduction peak corresponding to the catalytic reduction of hydrogen is visible at -1.35 V only upon addition of **2**. Direct reduction of TFA at the electrode was found to account for 20% of the total current at -1.35 V.

electrode is always a possibility, so it was necessary to compare CVs of TFA solutions with and without the presence of **2**. Control experiments demonstrated negligible background current from direct TFA reduction in acetonitrile (Fig. 31-32). However, control experiments in 1:1 water:acetonitrile showed a 18-20% contribution from direct TFA reduction to the total catalytic current (Fig. 33-34). This discovery led to correction of $i_c/i_p$ data by 20% in all 1:1 water:acetonitrile experiments to account for the background current. Regardless, it is clear that the catalyst utilizes the vast majority of consumed current for the proton reduction.

Scan rate experiments were performed to confirm that the redox species associated with the catalytic reaction were freely diffusing. Free diffusion in this case means that the species are not surface bound to the electrode, meaning they are homogeneous within the reaction solution. The Randles-Sevcik equation describes the relationship between peak current density and scan rate for freely diffusing redox species to be proportional in the following manner:[34]

$$i_p \propto \nu^{\frac{1}{2}}$$

CVs were collected at different scan rates for a solution of **2** in pH= 4 buffer solution to confirm this relationship (Fig. 35). The linear relationship between the square root of the scan rate and the peak current density confirm that the active redox species is indeed freely diffusing (Fig. 36). This allows the $k_{obs}$ to be estimated using the $i_c/i_p$ at high scan rates at which the catalytic process is not diffusion controlled.

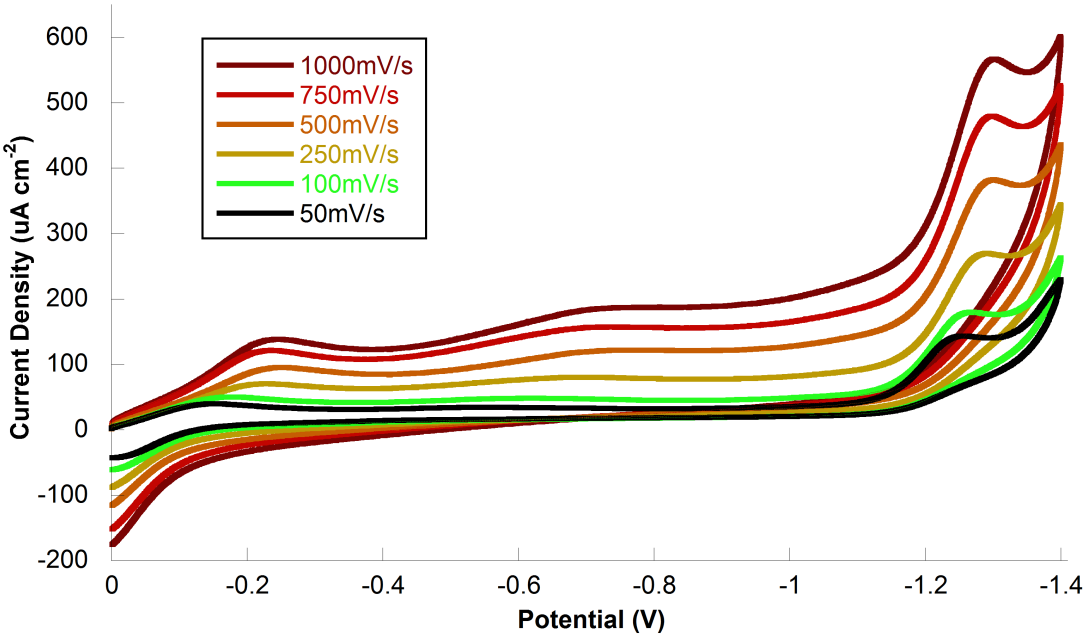


**Figure 35.** CVs of 1.0 mg **2** in 5 mL pH = 4 citrate-phosphate buffer solution from 0.0 to -1.4 V at various scan rates.

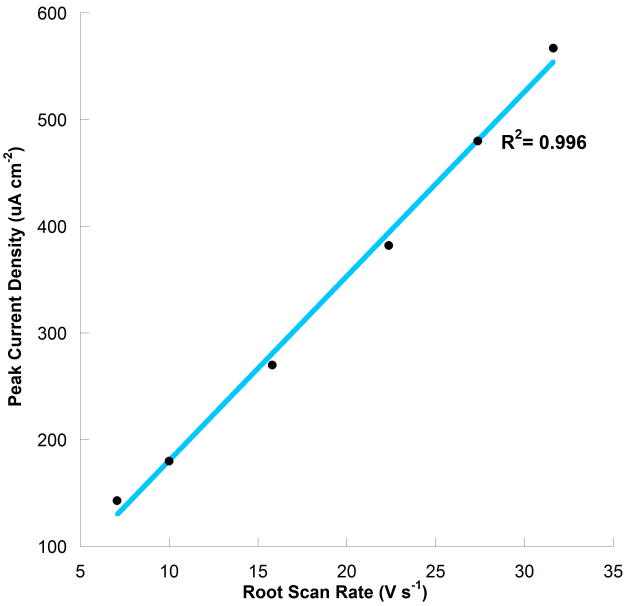


**Figure 36.** Peak current density vs. root scan rate for Fig. 32. A clear linear relationship exists ($R^2$= 0.996), indicating free diffusion of redox species at the electrode.

## Conclusion

An Fe(III) polypyridyl complex (**2**) was synthesized and characterized for feasibility as an electrocatalyst for proton reduction. X-ray diffraction of slow-diffusion grown crystals showed the complex to be a distorted octahedron, with a fairly strong Fe-O phenolate bond of particular interest. The complex was found to be soluble in both aqueous and organic solvents and paramagnetic.

Cyclic voltammetry revealed **2** to be an active electrocatalyst for proton reduction in a variety of solvent systems. In acetonitrile, **2** evolved hydrogen from TFA at a potential of -1.17 V vs. SCE, an overpotential of 660 mV. This catalytic rate for this reaction was determined to be 1200 $s^{-1}$ at a scan rate of 10 V/s. In 1:1 water:acetonitrile, the catalyst was found to be much more active, with a $k_{obs}$ of 3500 $s^{-1}$ calculated at a scan rate of 10 V/s. However, the catalytic reduction occurred at -1.32 V vs. SCE in this quasi-aqueous environment, an overpotential of 800 mV. **2** successfully reduced protons from aqueous citrate-phosphate buffer systems of pH= 3-6, but was unable to catalyze this reduction in more neutral buffer solutions. At a constant potential of -1.2 V vs. SCE in pH= 5 buffer solution, the catalyst achieved 23.0 turnovers over the course of 60 minutes with a Faradaic efficiency of 98%.

Cyclic voltammetry identified two separate reduction events occurring at the metal center during catalyst. The first reduction occurs more cathodic than the Fe(III)/Fe(II) reversible redox couple of **2** and was thus attributed to a protonation event followed by a one-electron reduction of the metal center. The second reduction is attributed to the catalytic reduction of hydrogen following a second one-electron reduction and protonation event. Thus the proposed mechanism of catalysis is either a

CEEC or CECE cycle. Pourbaix diagrams of **2** in pH= 3-8 citrate-phosphate buffer solutions confirms the existence of two separate one-electron reduction events during the catalytic cycle.

The iron catalyst reported compares extremely favorably to other iron electrocatalysts for proton reduction due to its high catalytic turnover rate and its stability in aqueous solutions.[10,14] However, the catalyst operates at a modest to high overpotential when compared to other similar catalysts. Thus, while **2** is a robust, highly active electrocatalyst, significant improvements can be made to increase its efficiency. Current efforts are being made to tune the electronics of the metal center to better facilitate reduction and protonation events in order to decrease the catalytic overpotential. This will be done by the addition of electron-withdrawing groups into the conjugated ligand scaffold in an attempt to draw electron density away from the metal ion. Other interests include synthesizing analogs of **2** containing Fe-S and Fe-P bonds to determine the effects that this may have on catalytic efficiency and stability. Eventually, an optimized electrocatalyst will be studied for integration into a molecular photocatalytic system.

## References


(1) United States Energy Information Administration. *International Energy Outlook 2013*. USEIA, **2013**.

(2) Wigley T. M.; Richels R.; Edmonds J. A. *Nature*. **1996**, *379*, 240-243.

(3) Lewis N. S.; Nocera D. G. *Proc. Natl. Acad. Sci. U. S. A.* **2006**, *103*, 15729-15735.

(4) Hirsh R. L.; Bezdek R.; Wendling R. *Peaking of world oil production: impacts, mitigations, and risk management*. DOE, **2005**.

(5) United Nations Development Program. *World energy assessment: energy and the challenge of sustainability.* UN, New York: **2003**.

(6) Barber J. *Chem. Soc. Rev.* **2009**, 38, 185-196.

(7) Vignais P. M.; Billoud B. *Chem. Rev.* **2007**, *107*, 4206-4272.

(8) Artero V.; Fontecace M. *Coord. Chem. Rev.* **2005**, *249*, 1518-1535.

(9) Eisenberg R.; et al. *J. Am. Chem. Soc.* **2009**, *131(26)*, 9192-9194.

(10) Rose M. J.; Gray H. B.; Winkler J. R. *J. Am. Chem. Soc.* **2012**, *134*, 8310-8313.

(11) McKone J. R.; Marinescu S. C.; Brunschwig B. S.; Winkler J. R.; Gray H. B. *Chem. Sci.* **2014**, *5*, 865-878.

(12) Thoi S. V.; Sun Y.; Long J. R.; Chang C. J. *Chem. Soc. Rev.* **2013**, *42*, 2388-2400.

(13) Ott S.; et al. *Bioinorg. Chem.* **2010**, *49*, 8033-8036.

(14) Berben L. A.; et al. *Inorg. Chem.* **2013**, *52*, 12847-12854.

(15) Mayilmurugan, R.; Visvaganesan, K.; Suresh, E.; Palaniandavar, M. *Inorg. Chem.* **2009**, *48*, 8771-8783.

(16) Felton, G. A. N.; Glass, R. S.; Lichtenberger, D. L.; Evans, D. H. *Inorg. Chem.* **2006**, *45*, 9181.

(17) Roberts, A. S.; Bullock, R. M. *Inorg. Chem.* **2013**, *52*, 3823-3835.

(18) Mayilmurugan R.; et al. *Dalton Trans.* **2010**, *39*, 9611-9625.

(19) Mayilmurugan R.; Visvaganesan K.; Suresh E.; Palaniandavar M. *Inorg. Chem.* **2009**, *48*, 8771-8783.

(20) Kanamori D.; Yamada Y.; Onada A.; Okamura T.; Adachi S.; Yamamoto H.; Ueyama N. *Inorg. Chim. Acta*. **2005**, *358(2)*, 331-338.

(21) Gagne R. R.; Koval C. A.; Lisensky G. C. *Inorg. Chem.* **1980**, *19(9)*, 2854-2855.

(22) Fourmond V.; Jacques P.; Fontecave M.; Artero V. *Inorg. Chem.* **2010**, *49*, 10338-10347.

(23) Saveant J-M.; Su K. B. *J. Electroanal. Chem.* **1984**, *171*, 371-379.

(24) McCrory C.; Uyeda C.; Peters J. C. *J. Am. Chem. Soc.* **2012**, *134*, 3164-3170.

(25) Ahn H. S.; Davenport T. C.; Tilley T. D. *Chem Comm.* **2014**, *50*, 3834-3837.

(26) Wiese, S.; Kilgore, U. J.; DuBois, D. L.; Bullock, R. M. *ACS Catal.* **2012**, *2*, 720-727.

(27) Nicholson, R. S.; Shain, I. *Anal. Chem.* **1964**, *36*, 706-723.

(28) Bard, A. J.; Faulkner, L. R. *Electrochemical Methods: Fundamentals and Applications*, 2nd ed.; John Wiley & Sons: New York, **2001**.

(29) Saveant, J. M.; Vianello, E. *Electrochim. Acta.* **1965**, *10*, 905-920.

(30) Saveant, J. M.; Vianello, E. *Electrochim. Acta.* **1967**, *12*, 629-646.

(31) Hoffert, W. A.; Roberts, J. A. S.; Bullock, R. M.; Helm, M. L. *Chem. Comm.* **2013**, *49*, 7767-7769.

(32) Bigi J. P.; Hanna T. E.; Harman W. H.; Chang A.; Chang C. J. *Chem. Comm.* **2010**, *46*, 958-960.

(33) Song W.; Chen Z.; Brennaman M. K.; Concepcion J. J.; Patrocinio A. O.; Iha N. Y.; Meyer T. J. *Pure Appl. Chem.* **2011**, *83(4)*, 749-768.

(34) Zanello P. *Inorganic Electrochemistry: Theory, practice, and application.* The Royal Society of Chemistry, **2003**.

(35) Youngblood, J. W.; Seung-Hyun, A. L.; Kobayashi, Y.; Hernandez-Pagan E. A.; Hoertz, P. G.; Moore, T. A.; Moore, A. L.; Gust, D.; Mallouk, T. E. *J. Am. Chem. Soc.* **2009**, *131(3)*, 926-927.

(36) McNamara, W. R.; Han, Z.; Alperin, P. J.; Brennessel, W. W.; Holland, P. L.; Eisenberg, R. *J. Am. Chem. Soc.* **2011**, *133*, 15368-15371.

(37) Knauf, R. R.; Brennaman, M. K.; Alibabaei, L.; Norris, M. R.; Dempsey, J. L. *J. Phys. Chem.* **2013**, *117*, 25259-25268.